Technological Aspects of Manufacturing and Numerical Modelling of Clinch-Adhesive Joints

Abstract The analysis of technological factors that influence the plastic forming of the clinch joint and its strength is described. Basing on literature date and authors' studies, it was found that quality and strength of the joint are mainly related to plastic deformation of joined sheets and sheets' adhesion on the joint interface. These conclusions determined the subsequent investigations of the clinching process. The clinch joints made of one or two different materials with diversified plastic and strength properties were experimentally tested. The basic samples were single overlap clinch joints with one clinch bulge. The joints mechanical response was analysed in the pull and peer tests. The obtained results showed the relation of the clinch joinability to the exponent of materials strain hardening curves. The good quality and good strength joints were obtained for materials with low value of strain hardening curve exponent 'n' in the range of about 0,14–0,22. The book includes also experimental results and numerical calculations of clinch joint forming process with different sheets' interface preparation (degreased, greased and separated by thin PTFE film). The investigations covered the effect of the above specified contact conditions on the clinch joint geometrical parameters and the shear strength. The obtained results showed crucial role of interface friction conditions, apart from geometrical parameters, on the joint shear strength. The hybrid joints combining clinching and adhesive bonding techniques were also investigated. Application of the hybrid clinch-bonded joints lead to the significant increase of the joint quality and strength. It was found that an adhesive plays the role of grease when the joint is clinched and then, after curing it causes great and advantages adhesion between sheets, stopping their displacement and bending. The book includes: (a) very wide experimental testing program with analysis of the obtained results, (b) advanced finite element numerical model of the hybrid joints behavior with application of 2 degradation processes: in the adhesive layer and the plastic adherends.

Introduction

Clinching is a sheet metal joining method without use any additional joining elements (e.g. [1–3]). This is an alternative joining method to traditional methods involving screws, rivets or welding. Riveting and screwing need a previous punching or drilling of the sheets, welding causes localized heating of the material, what leads to changes in the mechanical properties of materials. During clinching sheet metal parts are deformed locally with a punch and a die and an interlock is formed between the joining parts. The method is used to joining sheets of thickness between 0.2 and 4 mm and both sheets are not required to be of equal thickness [2].

Clinching is applied in automobile industry (particularly in certain parts of the vehicle body, as shown in Fig. 1, and in furniture and computer industries, in different kind household appliances as well as in ventilation and air conditioning systems. However, a prospective application of this technology in aerospace requires more attention. In particular, improvement of the pure clinching by additional application of the adhesive leads to creation of the so called hybrid joint— much more stronger, reliable and durable, e.g. [4, 5].

As an example of the clinching technique one can describe a mechanical interlock with the application of the TOX solution (TOX® PRESSOTECHNIK GmbH & Co. KG, Weingarten, Germany), Fig. 2. The required tooling set consists of: a punch, a die and a blank holder. The mechanical joining of two or more blanks (e.g. metal sheets) is only based on the accurate movement of the punch into the die. The sheet metals are deformed locally without the use of any additional elements.

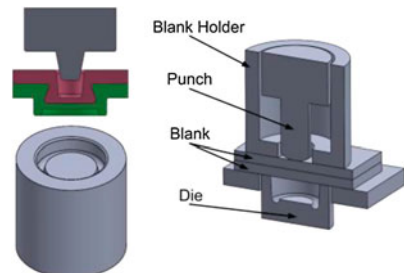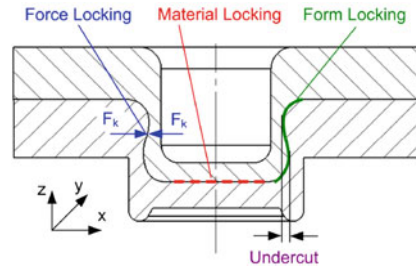Fig. 1 Clinch joints in a car bonnet

Fig. 2 The TOX clinching model

Fig. 3 Locking mechanisms of joining parts in clinching

In general, there is a substantial differentiation of clinching methods depending on the tool and clinching equipment makers. The clinch joint geometry can be round or square, during the process a cutting of the material and different number of stages can proceed. The equipment differentiation include: hand-powered machines, portable machines powered by hydraulic or pneumatic systems, self-standing hydraulic or pneumatic machines, and C-frames with an additional press.

The clinched joint strength is due to: force locking, material locking and "S" shape locking, Fig. 3. The quality of the clinching process strongly depends on precisely selected tools. The proper description of this process should include: tool geometries, parameter optimisation, and finite element analysis (FEA) simulation of the process (e.g. [6–14]).

In this book, specific requirements concerning the clinching process in industry (aeronautical, aerospace and automotive) are discussed. The basic modes of joints failure of clinched joints are described. There are several advantages and limitations in application of the clinching technique.

The advantageous properties of clinching technology and clinch joints are:

- lack of additional fastener,
- pre-drilling holes in joined elements in not required,
- no thermal influence on joined materials and their coating,
- joining different materials (including a multi-layer) with large differences in thickness,
- ergonomic for operation and easy for automation—e.g. no needs for pre-treatment,
- green assembly method—no fumes, emissions or high current,
- very good lifetime of the tooling,
- economically attractive—low capital and operation costs (lower 30–60 % in comparison to spot-welding technique).

All above makes the clinching technique very attractive for different assembly applications. But the process has limitations, too. The main limitations of the process are:

- the access to both sides of the joint is required,
- limited distance of the joint point from the edges of joined elements (because of C-frame constriction of equipment),
- weak gas and fluid leak tightness,
- weak prevention of rotation.

The disadvantage of the clinched joints in case of fastening of two or more pieces of materials can be the initiation of a corrosion process at interfaces of joined parts due to environmental factors: physical and chemical.

Future applications of clinching will require advances in quality and, among others things, combination with other processes, e.g., hybrid joining by clinching and adhesive bonding. The use of adhesive bonding, as the additional joining technique, should give better performances than the clinched joint alone. Therefore, the main subject of the book is a description of the new hybrid joining technology, i.e. clinch-adhesive joint. The idea of combining these two simple techniques, clinching and adhesive bonding, leads to numerous advantages in comparison to both simple methods. The hybrid joining:

- compensates for the disadvantages of two single techniques,
- allows a fixation of the joining materials (blanks) until the adhesive is cured,
- increases the joint strength of both, e.g. shear strength or peeling resistance,
- improves the pressure tightness and corrosion resistance.

The authors' own experimental and numerical results of joint strength and durability of different clinch-adhesive joints made of different materials are described to illustrate the potentiality of this technique. The failure mechanisms associated with the clinch-adhesive technique are visualized experimentally.

The book contains description of the complex finite element (FE) model which incorporates 2 damage processes developing in:

- plastic adherends,
- adhesive layers.

The model allows for detailed description of the clinching process and further analysis of active loading process of the joints.

Finally, some examples of applications are discussed and conclusions are formulated.

Clinching Technology

Clinching consists in localized cold forming of joined materials with a punch and a die (Fig. 4). The result is an interlocking friction joint between two or more sheet materials. This joining technology is applied in manufacturing thin-walled structures in the automotive and white goods industries, but the difficulty is in relatively low strength of the clinch joint. The force necessary to separate the sheets depends mainly on the joint geometrical parameters and the friction conditions in the sheets' interface.

The clinching process proceeds in several stages, as illustrated in Fig. 5 for a circle shape tools geometry. The thickness of the joined sheets ranges from 0.4 to 8 mm for mild steel. Typically the sheet thickness varies from 0.2 to 4 mm, however, there is no requirement of equal thickness of joined sheets. The necessary level of force to create clinching varies between 10 and 100 kN.
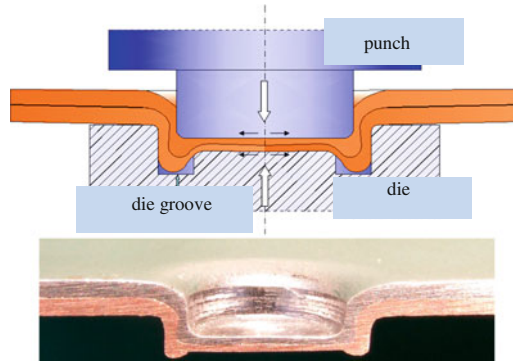
Fig. 4 Scheme of the clinching process and picture of longitudinal section of steel–copper clinch joint
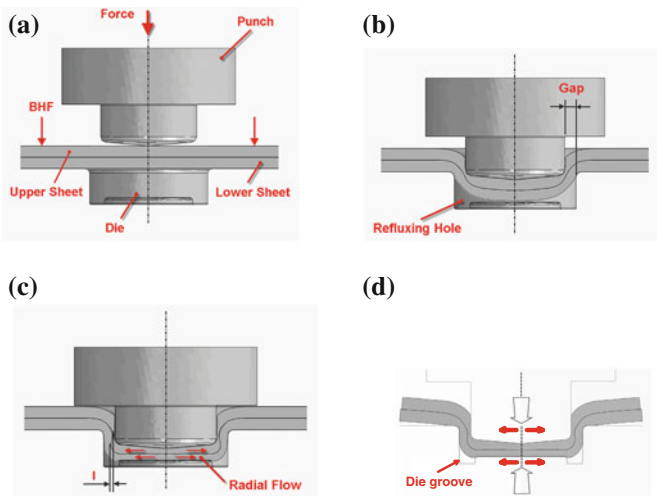

Fig. 5 Scheme of the clinching process and picture of longitudinal section of steel–copper clinch joint

The joining process during clinching is caused by metal flow of metallic sheets. The first stage begins when the joined sheets are subjected to blank holder force (BHF), Fig. 5a, b. The joined sheets adhere closely to the surface of the die and to the central bottom point of the punch. It is very important that the area of the punch (cross section) should be approximately equal to 65–70 % of the area of the die to create clinching without local incision. In the next step the punch moves downwards and the process of plastic deformation starts in the metallic blank sheets, Fig. 5b. The deformation is influenced by the friction coefficient between the punch surface and the metallic blanks and is continued until the metal reaches the impression of the die. In the next stage of the clinching process the joined sheet blanks gradually fill the die impression and finally the extrusion of the metal sheets takes place, Fig. 5c. The metal begins to flow and the straight walls of the joint are

subjected to a thickness reduction (due to compression) and creation of a specific "S" shape (form locking of the blanks). Moreover, the bottom part of the blanks flow in the radial direction due to the punch pressure. Material locking begins with continuous reduction of the thickness of the sheets and the die grooves are filled by extruding metallic sheet materials (Fig. 5c, d).

During the clinching process, mainly two operations take place: deep drawing and compression. The deep drawing results in sheets' two-dimensional stretching when a local hollow cavity is formed and it causes the reducing of sheets' thickness. The total thickness of joined sheets is reduced to a fraction of their initial thickness in the joint bottom, with typical reductions of the order of 60 % [3]. The compression leads to a radial movement of the sheets' material and to the filling of grooves placed in the die, as shown in Fig. 4.

The final geometry of the clinched joint is illustrated in Fig. 6 with important features of the joint [4, 5]. Generally the clinch joint is characterized by the following parameters: the axial thickness of the sheets "x", the thickness of the upper sheet "th" (also called the nick or neck thickness) and the clinch lock (undercut) "cl". The clinched joint strength mainly depends on the neck thickness and the clinch lock [6]. A small clinch lock cl leads to a low joint strength because of pulling out the upper sheet from the lower sheet (because of the weak interlocking). A thin neck can cause fracture of the upper sheet. Increasing both th and cl parameters should improve the strength of the mechanical clinched joint. Although the static strength of clinched joints is lower than that of other joints (e.g., pressure welded joints), the fatigue strength is comparable to that of other joints [6]. Nowadays, many researches are looking for appropriate combination of clinching tools to obtain the maximum load under shear test of the clinched joint [e.g. 4–7].

Generally one can distinguish 2 techniques of press joining technology:

1. single-stroke technique, Fig. 7,
2. double stroke clinching, Fig. 8.

The first technique was elaborated for several technological variants depending on industry requirements, e.g. [8], Fig. 7.
Figure 7a presents the first set of tools, which is composed of a few moving die parts. During clinching, the die parts are closed, forming the die impression. After processing, the die parts open and a very strong joint is created. This technology can be applied to metallic sheets with a thickness of not more than 3 mm. Much
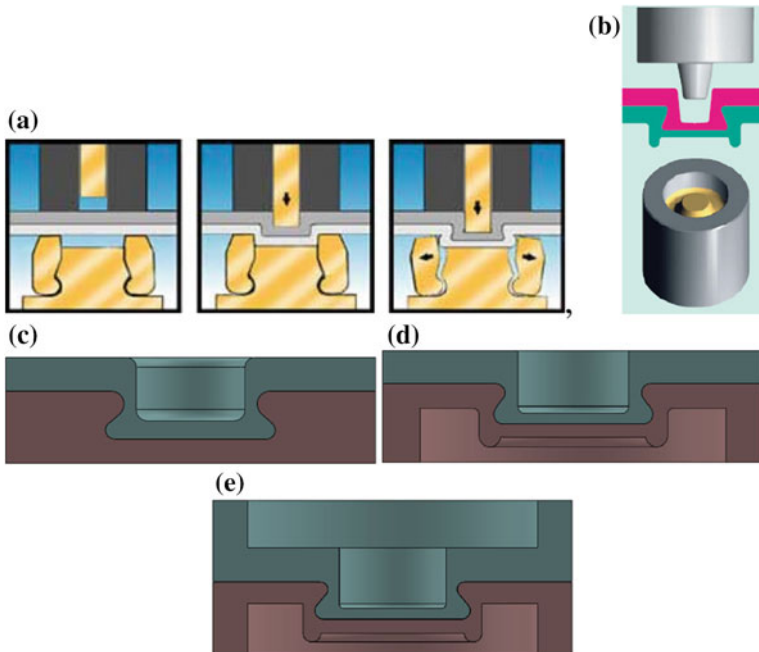
Fig. 6 The clinched joint parameters
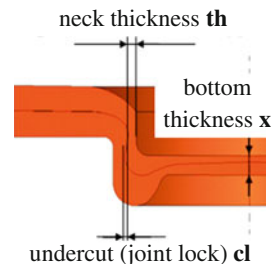
Fig. 7 Single-stroke techniques of clinching: **a** divisible-style die press joining, **b** straight-wall-style solid die, **c** single punch, **d** flat point joint technology, **e** plank press joint technology
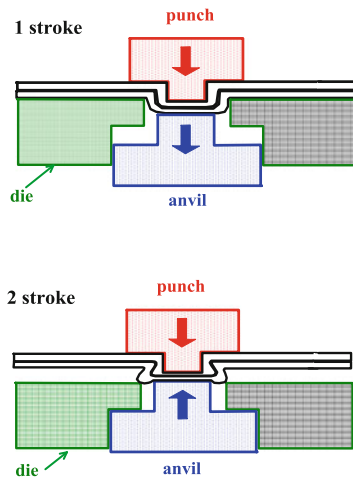

Fig. 8 Double-stroke technique by ATTEROX

simpler technology is the application of a straight-wall-style solid die, Fig. 7b. The advantage of this technique is its simplicity and durability.

In case of joining metal sheets of different thicknesses, the single—punch press joint technology is appropriate, Fig. 7c. The upper sheet should have a thickness of not more than 2 mm, whereas the bottom one—not less than 6 mm. With this technique it is not necessary to use any die. Single-punch is enough to form a good quality joint. When the upper surface of the clinched materials need to be flat—without any bulge—the flat point press joint technology can be used, Fig. 7d. This method is useful for a joint of materials with different thicknesses.

The last technique is plank press joint technique for joining very thick elements (plates with a thickness higher than 4 mm), Fig. 7e.

Double-stroke clinching is the other interesting unique clinching method proposed by ATTEROX (ATTEROX Tools S.A., Renens/Lausanne, Switzerland), Fig. 8. The materials to be joined are pushed into a rigid die with the movement of a punch. In the first stroke, the punch is active and creates a preform of overlapping sheets, whereas the anvil at the bottom of the die is held in place only by a weak spring, giving free way for the movement of the punch. During the second stroke the anvil is locked mechanically and the preform is then squeezed between the punch and the anvil outside of the rigid die, creating a rivet–like joint.

In general, there are two experimental methods of measuring the strength of a clinch joint: "pull" (tensile–shear) and "peel" (peel–tension), Fig. 9. For a clinch joint, the pull method gives almost always higher strength than peel. Both methods are checked in a tensile test. In the pull method the joint shearing strength is determined, whereas in the peel mode the axial strength. The strength of a clinch joint depends essentially on four major factors:

- type of material,
- material thickness,
- clinch point size,
- material surface condition.

The type of joined materials is very important for the clinch joint strength. The geometry of forming tools should be matched to the mechanical properties of joined materials. The shear strength of clinch joints obtained for pairs of different materials, made with the same clinching tool arrangement, are shown in Figs. 10 and 11, [9]. As it can be seen, for the same pair of materials two different values of shearing strength is obtained. The strength of joint is higher when the "stronger" material is on the punch side (upper sheet) and the "weaker" on the die side (lower sheet), e.g.
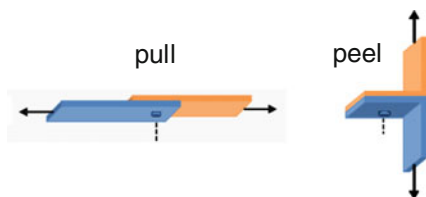

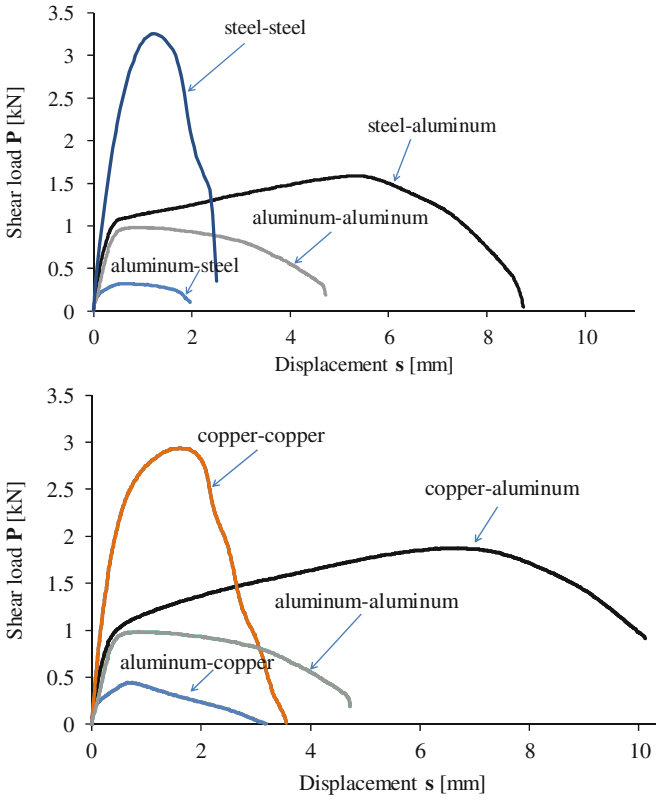**Fig. 9** Test methods of clinched joint: pull and peel

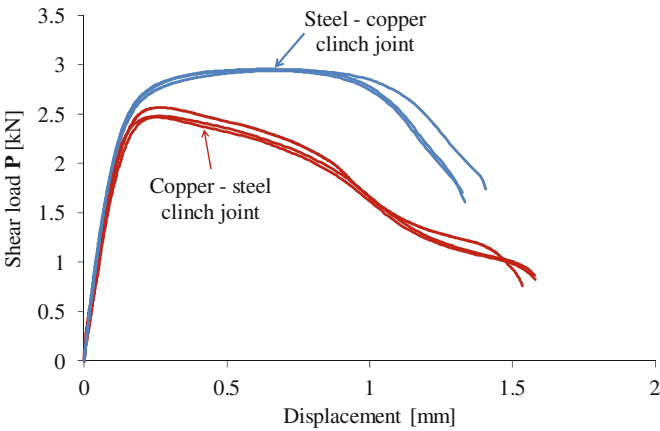**Fig. 10** Typical clinched joint shear characteristics obtained for different materials

Fig. 11 Shear characteristics of steel and copper clinch joint

compare strength of aluminum–steel and steel–aluminum joints. As it was shown by Abe et al. [10], when the strength of the lower sheet increases, the amount of interlock decreases due to large flow stress of the lower sheet.

Increase of the total sheet thickness causes the increases of the clinch joint strength. As in other mechanical joining methods, a larger diameter of a clinch joint involves a greater joint strength. The material surface condition influences on the clinch joint strength; a dry surface gives a stronger joint than an oiled or greased one, however, in case of steel sheets these effects are relatively minor while they have considerable influence in aluminum sheets.

Numerical simulations of the clinch joint forming process by the FEA (section "Numerical Model Applied for Modelling of Simple and Hybrid Joints") show that the most deformed region is the side wall of the joint (Fig. 12). This side wall region is very important for the clinch joint strength. In this region, the high level of strain-hardening of sheet metals occurs, which increases the mechanical strength of the joint.

As it is shown in Fig. 13, the deformation of the upper sheet in the neck can reach a joined material limiting strain or be too small to form the joint lock. This may cause two different modes of the clinch joint failures under loading: breakage of material in the neck or opening as a press-stud, Fig. 14.

The response of the clinched joint to shearing is presented in Fig. 15. One can notice bending of the punch side material which corresponds to the experimental results. The test generates stress concentrations on one side of the clinch cavity and when the relative displacement of the sheets is sufficiently high, the plastic bending of the punch side material causes separation of sheets.
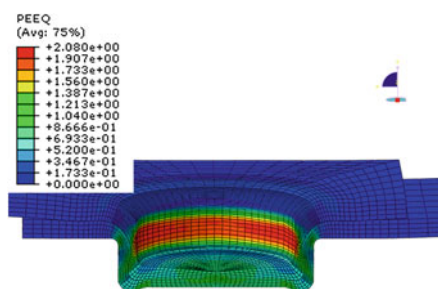

Fig. 12 Equivalent strain after clinching at steel–copper joint (MES results of steel–copper clinching process, punch stroke 3.8 mm)
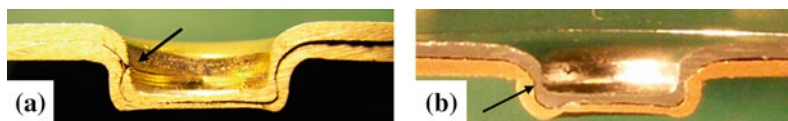

Fig. 13 Defects of clinch joint: **a** excessive thinning of upper sheet (small neck *th*), **b** small folding of sheet's interface (small joint lock *cl*)
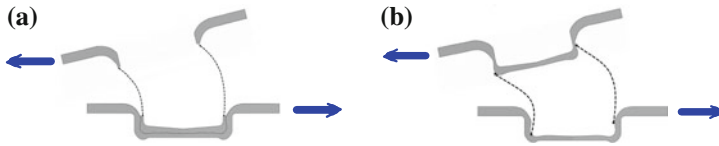
Fig. 14 Failure modes of clinched joints: **a** neck fracture mode, **b** press-stud fastener mode

Ability to Clinching

Clinching can be used to joining different metallic materials. The only restriction are their plastic properties. However some plastic materials, with good ductility, do not conform durable clinch joint. Low shear strength of clinched joints was obtained for such material like CuZn37 brass. High-alloy chrome-nickel stainless steel X5CrNi18–10 did not create a durable clinch joint; there was no clinching effect in the deformation area. These both materials are featured by high strain hardening phenomena during plastic deformation. So, it should be taken into account the strain hardening properties of materials subjected to clinching.

The studies of strain hardening phenomena on the clinch ability were realized on such materials like: 2024 aluminium alloy, pure aluminium 1070, ETP-copper, CuZn37 brass, low-carbon steel DC4, non-alloy quality steel C45, structural alloyed —chrome–vanadium spring steel 50CrV4, structural alloyed—heat-treated chrome–manganese–silicon steel 30CrMnSi and steel X5CrNi18–10. Clinching of these materials was preceded by uniaxial tensile tests of base materials to determine their work-hardening curves (Fig. 16). The flow curves were described by Swift equation:

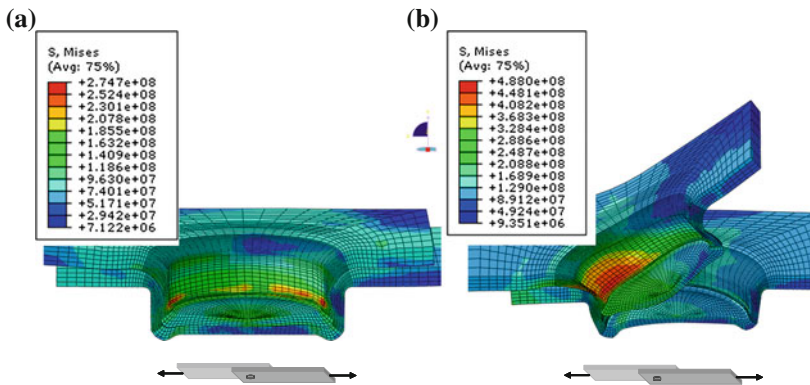$$\sigma = K(\varepsilon_{o} + \varepsilon)^{n}, \tag{1}$$

Fig. 15 FEA results of shear (pull) test of steel–copper clinch joint: **a** sheet displacement 0.16 mm, **b** sheet displacement 3.16 mm
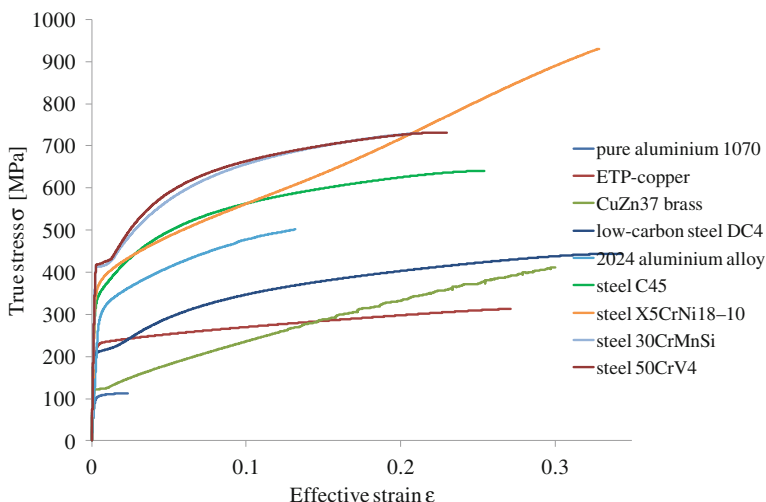
Fig. 16 Tensile characteristics of tested materials

where:

K is the strength index,
n is the strain hardening exponent,
ε_o is a prior plastic strain,
ε is a equivalent plastic strain

Shear curves obtained in the tensile tests of clinch joints of tested materials are shown in Fig. 17. As it can be seen the strongest clinch joint was obtained for constructional steels (30CrMnSi, 50CrV4 and C45) and the weakest one for pure aluminium (1070). Steel grade DC4 shows mean shear load of clinched joint but the shear curve is very "long". It means that this joint is characterized by the highest energy absorbed during shear when compared to other tested materials (Fig. 18). The results of experiments are summarized in Table 1, where the test materials are aligned vertically for the sake of the strain hardening exponent n. As it was mentioned above stainless steel X5CrNi18–10 and CuZn37 brass, are not a clinchabele materials, as well as aluminium alloy 2024 after solution heat treatment. These materials are characterized by high value of strain hardening exponent n. On the other hand, materials that form high strength clinch joint, i.e. 30CrMnSi, 50CrV4, C45, DC4 and ETP-copper, reveal low value of n exponent. The mean n value for these materials is equal $n = 0.174$, as it is shown in Fig. 19 as the "region of strong" clinch joint. Exception to this rule seems to be pure aluminium 1070 (low n value and low clinch joint strength). But when compare the maximal shear load of clinch joint with material tensile strength, aluminium 1070 and 30CrMnSi steel have comparable clinch joint strength.
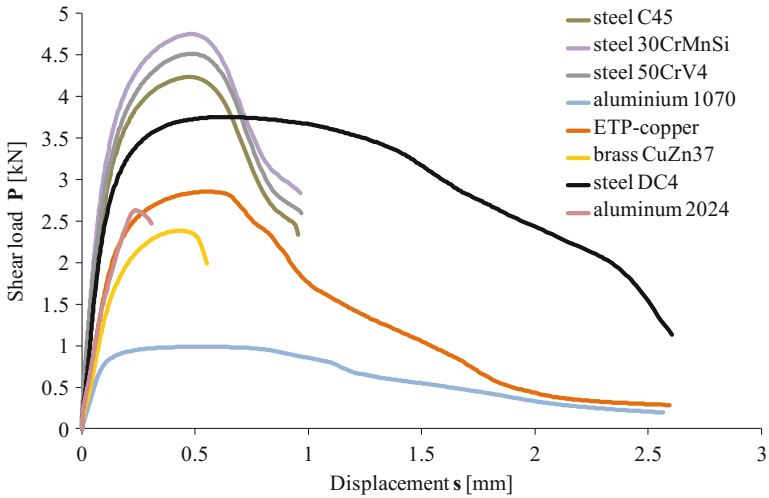
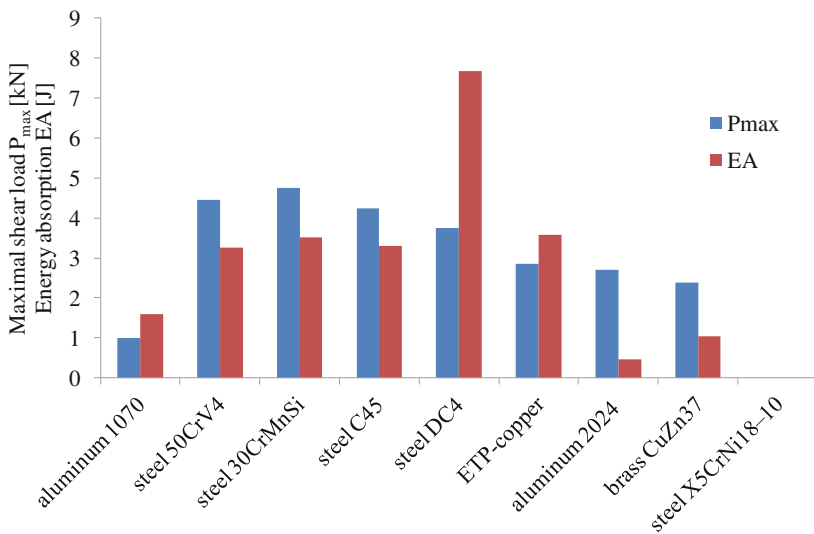**Fig. 17** Shear curves of clinched joints obtained for tested materials

Fig. 18 Strength properties of clinched joints for different kind of joined materials

The major conclusions resulting from own experiments can be formulated as follows:

- clinching can be used for effective joining of wide range mechanical properties metallic materials, e.g. low carbon steel and constructional alloy steel, characterized by low and high mechanical properties,

Table 1 Flow curve parameters and strength properties of clinched joints of tested materials

| Material	Strength coefficient K (MPa)	Strain hardening exponent n	Maximal shear load P_{max} (kN)	Energy absorption EA (J)
Aluminum 1070	127	0.03	0.99	1.60
Steel 50CrV4	902	0.14	4.46	3.26
Steel 30CrMnSi	932	0.15	4.75	3.51
Steel C45	804	0.17	4.23	3.31
Steel DC4	546	0.19	3.75	7.68
ETP-copper	395	0.22	2.85	3.58
Aluminum 2024 (solution heat treatment)	648	0.34	2.7	0.453
Brass CuZn37	816	0.64	2.38	1.03
Steel X5CrNi18–10	1671	0.75	–	–
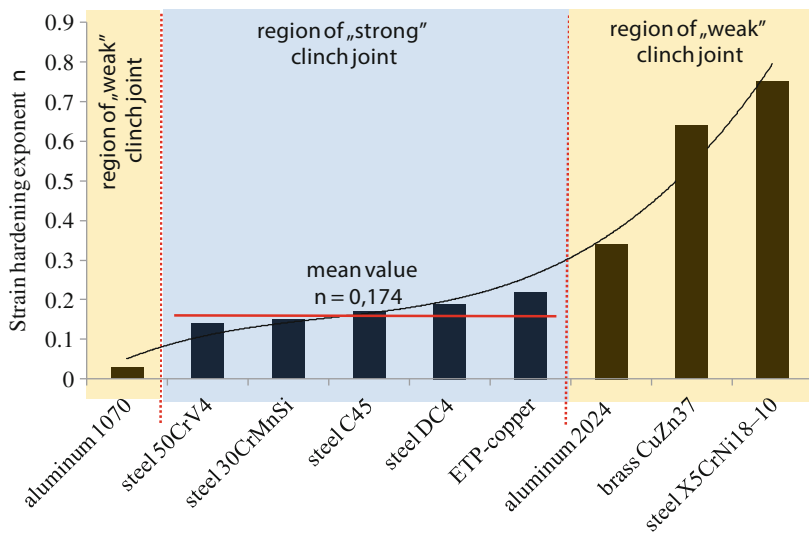
Fig. 19 Strain hardening exponent versus material type

- strain-hardening exponent n can be used as clinch joinability criterion; high value strain-hardening exponent n is not favorable for clinch joint forming; high strength clinch joint can be manufactured when low values strain-hardening exponent materials are clinched.

Influence of Contact Conditions on Forming Process and Strength of Clinched Joints

The force necessary to separate the sheets depends mainly on the joint geometrical parameters and the friction conditions in the sheets' interface. Friction forces have strongly influence on the clinch joint forming process. This concerns both friction forces acting on the contact surfaces between sheets and tools and friction forces acting between joined sheets in the interface surface. Their role changes during joint forming process, i.e. during the first drawing stage and during the second compression stage. When drawing is realized joined sheets undergo biaxial tension and their thickness decreases. Friction between punch and upper sheet and between sheets in their interface surface causes strain redistribution; thinning of sheets in the side wall of indentation, especially on the edge between side wall and bottom. When lower sheet comes into a contact with the die bottom starts the compression stage. The joined sheets are squeezed between punch and die, the thickness of the indentation bottom decreases and sheet materials flow radial and circumferential. The forming process is strongly related to friction conditions.

Influence of the Friction Coefficient

The effect of surface friction on clinching process is not be described in literature because in industry sheets are normally joined without the prior cleaning of surfaces [3]. But sheet surfaces, after manufacturing process and storage, are often covered with dust, dirt, grease, oil, oxide films, rust inhibitors. All these contaminants, even at a microscopic level, change the contact conditions between sheets and could influence on the clinch joint strength. It was observed by authors of this work, when testing hybrid clinch adhesive joints as described in [11–14], that the tensile strength of a clinch joint of raw sheet materials compared to the clinch joint of sheets with cleaned (abraded and degreased) surfaces, differed a little. Surface preparation is the most important for a good quality adhesive joint, because adhesives should strongly adhere to surfaces, but it seems to be the very important thing for making a good quality clinch joint too.

Additionally, numerical simulations of the clinch forming process take into account the friction, mainly between forming tools and joined sheets, therefore its influence on the geometrical parameters of the clinch joint is normally evaluated (e.g. as shown in [5]).

Influence of friction conditions in the clinch joint interface on the joint strength was experimentally investigated. Electrolytic copper Cu-ETP and low carbon steel DC4 were used as the sheet materials in preliminary tests. This materials' choice was motivated by good ductility of joined metals and good visualization of the joint intersection (red copper and gray steel). Three grades of structural steel were used in the further tests, i.e. non-alloy C45 steel, structural steels: 30CrMnSi and 50CrV4.
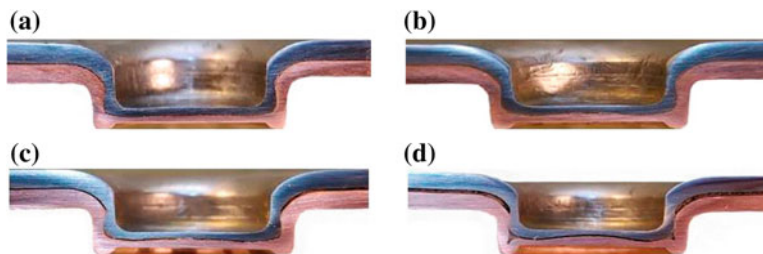
Fig. 20 The longitudinal sections of steel–copper clinched joint: **a** degreased by acetone the sheets contact surface, **b** graphite grease in the sheets contact surface, **c** thin PTFE tape in the sheets contact surface, **d** thick PTFE tape in the sheets contact surface

These steel grades have wide range of applications in manufacturing industry, e.g. grade 30CrMnSi, construction alloy steel—for hardening and tempering, is used in the construction of heavy machinery and medium to heavy duty parts, which work under great load at temperatures up to 150–200 °C, and the riveted part of a structure, and the seamless pipes used in aviation, for all kinds of components. Thickness of all materials used in the tests was equal 1 mm.

The preliminary tests concerned clinched joints with different friction conditions on the sheet's interface. The lap joints were clinched with (Fig. 20):

- degreased interface surface,
- graphite grease in interface surface,
- thin PTFE film in interface surface (thickness 0.05 mm),
- thick PTFE film in interface surface (thickness 0.15 mm).

The effects of the joint quality were examined on the three geometrical parameters (Table 2) i.e. the neck thickness, the clinch lock and the bottom thickness and on the load and energy criteria determined in tensile test as it is shown in Fig. 21 (the maximum tensile force "P_{max}" and energy absorption "EA").

The results shown in Fig. 20 and Table 2 confirmed the importance of friction interface conditions on the clinch joint strength. Decreasing friction causes increasing in the joint lock but there are differences when using PTFE tape and when graphite grease. Applying graphite grease benefits in clinch joint strength as

Table 2 Geometrical and mechanical parameters of steel–copper clinched lap joints

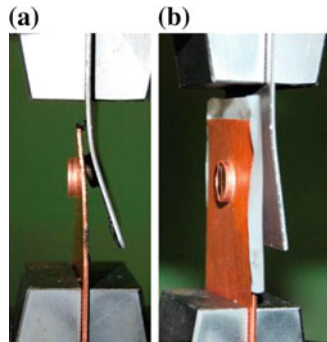| Adherends' interface conditions	Thickness of the side wall th (mm)	Joint lock cl (mm)	Thickness of the clinched bottom x (mm)	Maximal shear load P_{max} (kN)	Energy absorption EA (J)
Degreased	0.49	0.14	0.98	3.3	8.2
Graphite grease	0.52	0.17	0.91	3.4	8.7
Thin PTFE tape (thickness 0.05 mm)	0.55	0.20	0.97	3.0	5.9
Thick PTFE tape (thickness 0.15 mm)	0.49	0.16	0.90	1.7	3.6

Fig. 21 Examples of clinched joints in the shearing test: **a** steel–copper clinched joint with graphite grease in the sheets contact surface, **b** steel–copper clinched joint with PTFE thick tape in the sheets contact surface

distinct from applying Teflon tape when strength decrease was observed. And it should be noticed that when applying thicker film, the strength decreasing is much more significant.

The experiments were continued but only three different contact conditions in the lap interface were used:

- abraded and degreased,
- greased by paraffin wax,
- separated by 0.05 mm polytetrafluoroethylene (PTFE) film.

The paraffin wax was used instead of graphite grease because of greater density and viscosity. Thick PTFE film (thickness 0.15 mm) caused bending of sheet material in the die groove instead of upsetting and therefore this lap contact variant was omitted in subsequent tests.

The experiments were done for two clinch joint cases: steel–copper and copper–steel joints. The results of strength testing of the steel–copper clinched joints are shown in Fig. 22 and Table 3. The joint is strongest for specimens with lap surfaces covered by paraffin wax and weakest for specimens when lap surfaces were separated by PTFE film, despite having bigger the joint lock *cl* for the second one (Table 3). Specimens with lap surfaces abraded and degreased revealed medium shear strength.

The same shear strength relations were obtained for the copper–steel clinched joint shown in Fig. 23 and Table 4. The failure mode observed for these two types of the joint is the same, too; sheets are separated by bending the sheet on the punch side, without any fracture. But the load–displacement curves differ for these both types of the joint. The peak load, for the steel–copper clinched joints is in the middle of the recorded displacement range (Fig. 22) and for the copper–steel
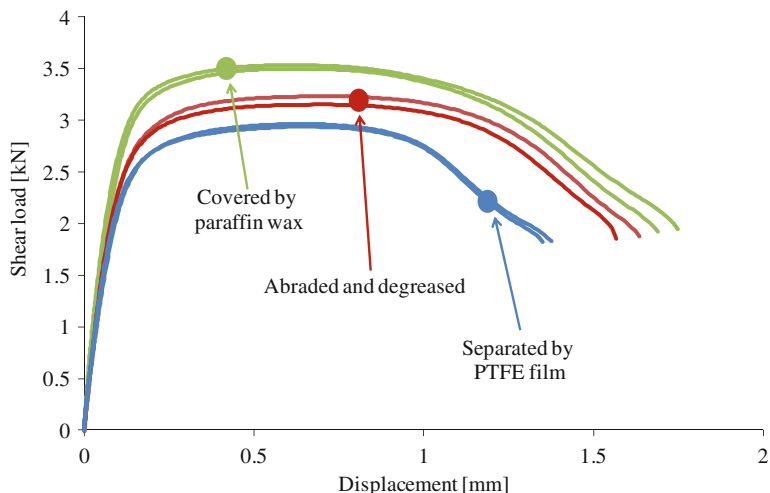
Fig. 22 Experimental load–displacement curves obtained for steel–copper clinched joints with different interface conditions in the lap area

Table 3 Geometrical and mechanical parameters of steel–copper clinched joints

Specimen type	Thickness of the side wall th (mm)	Joint lock cl (mm)	Thickness of the clinched bottom x (mm)	Maximal shear load P_{max} (kN)	Energy absorption EA (J)
Lap surfaces covered by paraffin wax	0.49	0.17	0.89	3.46	5.23
Lap surfaces abraded and degreased	0.5	0.16	0.94	3.25	4.51
Lap surfaces separated by PTFE film (thickness 0.05 mm)	0.5	0.19	0.92	2.97	3.51

clinched joint (Fig. 23) it is placed in the beginning of the shear curve. It means that for the first mentioned joint the strain hardening phenomena occurs, while for the second one, after elastic strain range the weakening of the joint takes place.

As it can be seen in Tables 3 and 4 and in Fig. 24, the joint lock cl is greater for the copper–steel clinched joints than for the steel–copper clinched joints, although the shear strength for the first joints is smaller than for the second ones. So, it could be concluded, that clinched joint strength is not only related to the joint geometrical parameters and joined material properties but to the interface mechanical adhesion between joined sheets, too.
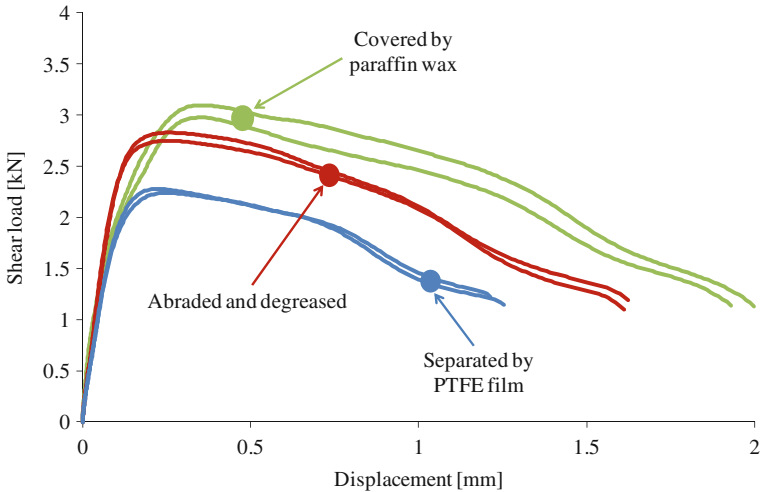
Fig. 23 Experimental load–displacement curves obtained for copper–steel clinched joints with different interface conditions in the lap area

Table 4 Geometrical and mechanical parameters of copper–steel clinched joints

Specimen type	Thickness of the side wall th (mm)	Joint lock cl (mm)	Thickness of the clinched bottom x (mm)	Maximal shear load P_{max} (kN)	Energy absorption EA (J)
Lap surfaces covered by paraffin wax	0.46	0.2	0.87	3.04	4.43
Lap surfaces abraded and degreased	0.45	0.21	0.92	2.79	3.39
Lap surfaces separated by PTFE film (thickness 0.05 mm)	0.48	0.21	0.85	2.26	2.2

Numerical Analysis of Clinching Process for Different Values of the Friction Coefficient

The FEA investigations concerned the simulations of clinching process and the shear strength of the clinched joint. The strain and stress distribution was determined. In all numerical tests the same material parameters (copper, steel as shown in Table 5) were assumed, friction between tools and sheets $\mu = 0.1$ (as it was assumed by de Paula et al. [5]) and boundary conditions.

Four different friction conditions in the interface surface between the adherends were assumed, i.e. $\mu = \{0; 0.1; 0.2; 0.3\}$. The FEA results of clinching process for these conditions are shown in Figs. 25, 26, 27 and 28. The FEA results differ from experimental ones; in some regions of the side surface of the joint the limit strain
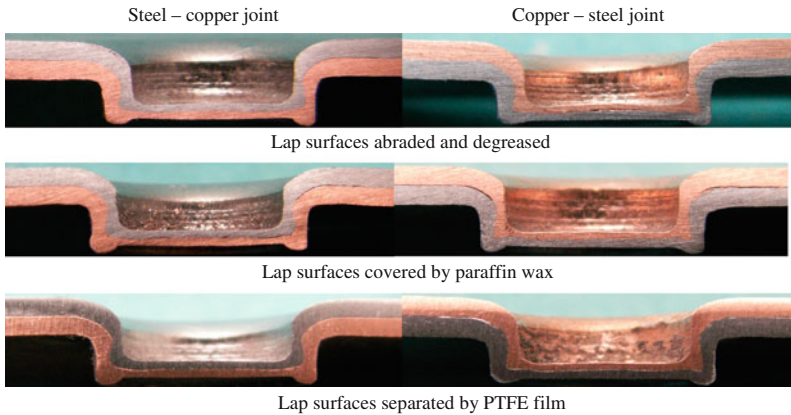
Steel – copper joint   Copper – steel joint

Lap surfaces abraded and degreased

Lap surfaces covered by paraffin wax

Lap surfaces separated by PTFE film

Fig. 24 Intersections of steel–copper and copper–steel joints obtained with different interface conditions in the lap area

Table 5 Properties of sheet materials used in FEA

Sheet material	Young's modulus E (GPa)	Poisson's ratio v	Density ρ (kg/m^3)	Hollomon's coefficients	
				K (MPa)	n
Steel	210	0.3	7800	546	0.19
Copper	127	0.3	8940	395	0.22

was obtained; it was especially substantial when clinching without friction (Fig. 25). This phenomenon was not been observed in any case of real process realized experimentally (clinching with PTFE film between lap surfaces is most close to condition $\mu = 0$).

The best clinching result was obtained when friction between sheets was equal to $\mu = 0.3$. In this case the smallest equivalent strain in the joint neck (Fig. 28) and the best shear test simulated result (Fig. 29) were calculated. For the equivalent Huber–von Mises stress 580 MPa, only for the joint with $\mu = 0.3$ the fracture in the neck is not observed.

Experimental Investigations of the Interface Roughness Influence on the Joint Strength

The experimental research was continued with three grades of structural steels. For each material the stress–strain relationship was determined (Figs. 30, 32, and 34,) and profile roughness parameters (Roughness Average—R_a and Roughness Height—R_z) for sheet surface were measured (Figs. 31, 33 and 35). The Taylor

Fig. 25 Distribution of effective plastic strain in the clinch joint intersection at three following stages of formation process when assuming lack of friction $\mu = 0$ (*white circles* mark the regions of net destroying, *grey arrow* shows the sequence of the process stages)
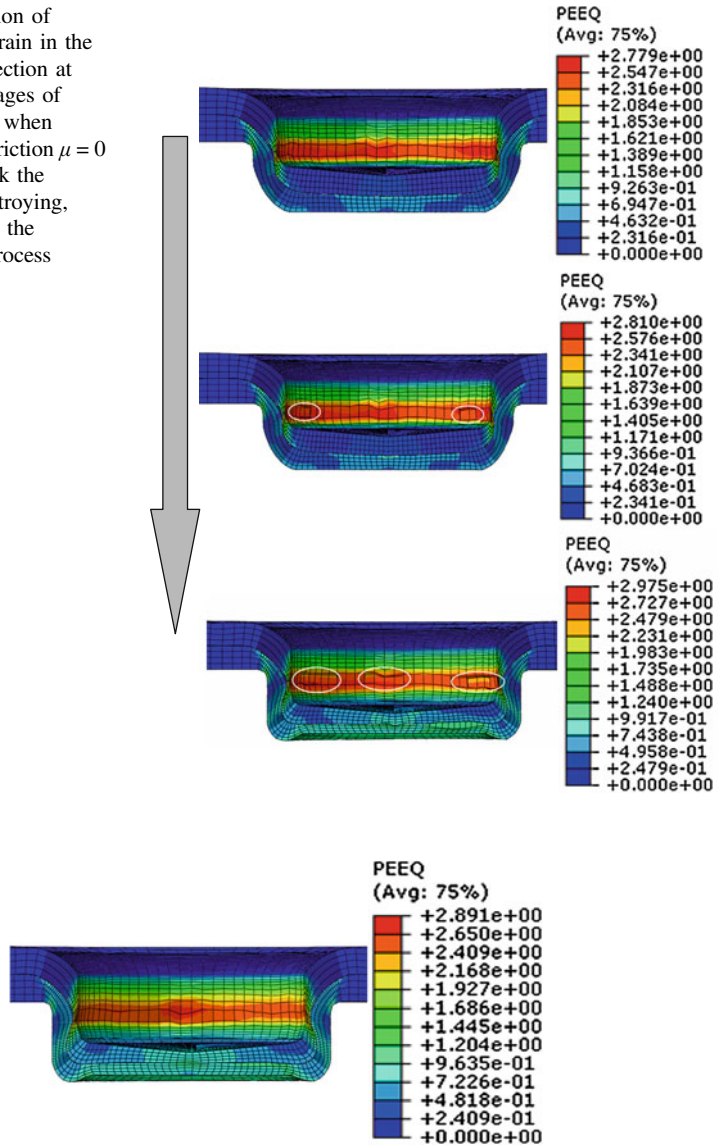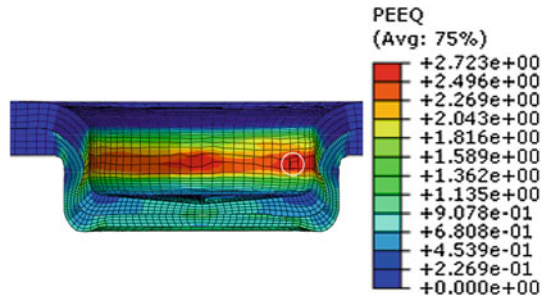

Fig. 26 Distribution of effective plastic strain in the clinch joint intersection when assuming friction conditions $\mu = 0.1$

Hobson surface profilometer Surtronic 25 was used to measure the surface roughness parameters. As it can be seen, the surface roughness of tested materials differs considerably, for steel 30CrMnSi is big ($R_a = 2.27$ μm), while for steel 50CrV4 it is very small ($R_a = 0.29$ μm).

Fig. 27 Distribution of effective plastic strain in the clinch joint intersection when assuming friction conditions $\mu = 0.2$
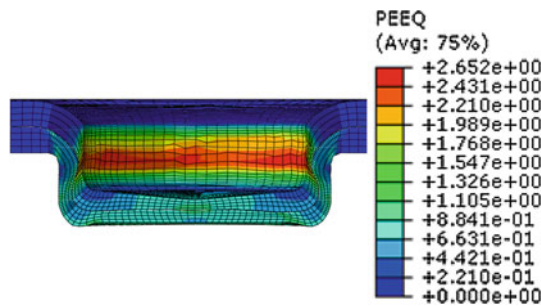

Fig. 28 Distribution of effective plastic strain in the clinch joint intersection when assuming friction conditions $\mu = 0.3$

Before clinching the lap surfaces of each strip were grinded and then washed by acetone. The abrasion of the lap surfaces was made by hand-held grinding machine with abrasive paper gradation 150. The surface pictures and roughness profile parameters after such preparation are shown in Fig. 36 for C45 steel. Grinding of the rest materials caused the roughness of their lap surfaces on the same level.

The shear tests results of clinched joints obtained for these materials are shown in Figs. 37, 38 and 39. Inserting the PTFE film in the lap interface do not increase the clinch joint strength; in case of all tested materials the joint strength is smallest. But applying PTFE film can correspond to friction condition $\mu = 0$ in the lap interface and neutralization the mechanical adhesion between sheet surfaces in the joint, so the strength of these joints results only in the plastic clinch of sheets. As it can be seen in Table 6 the shear strength (~ 4.2 kN) and absorption energy (~ 3.0 J) for this kind of clinch joint are almost the same for these three tested steel grades.

Another contact conditions are observed when clinching raw sheet materials as they are accessible on commercial market, with different surface contamination. The shear strength of these specimens with raw, not modified, lap surfaces correspond to joint strengths as they are manufactured in industry. In this case, the

Fig. 29 FEA results of the clinch joint pull test for assumed different friction conditions
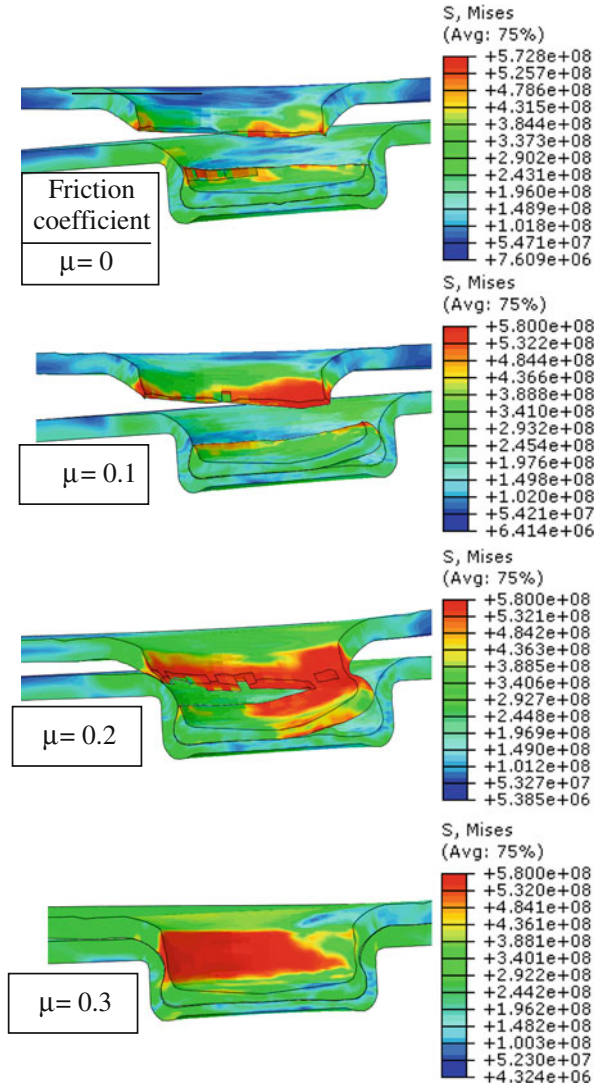
differentials of surface roughness are observed for tested steel sheets; smooth contact surfaces of C45 and 50CrV4 steel grades and rough contact surface of 30CrMnSi steel. It is a reason of different correlation between shear curves of the clinch joints obtained for 30CrMnSi steel. Diversification of shear strengths between clinch joints with raw lap surfaces, cleaned lap surfaces and lap surfaces covered by paraffin wax are small; strength curves, recorded for these three joint conditions, overlap one with another.

Essential increase of the clinch strength is observed, for C45 steel (Fig. 37), when the lap surfaces are cleaned (grinded and degreased); the clinch strength for
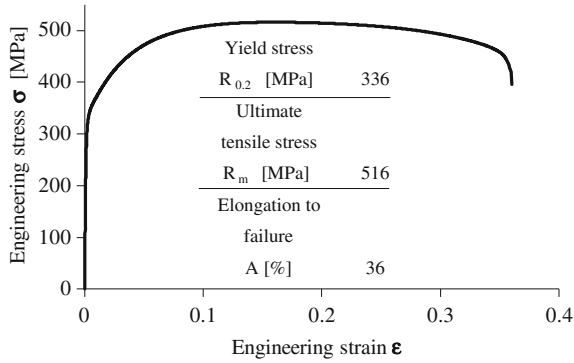
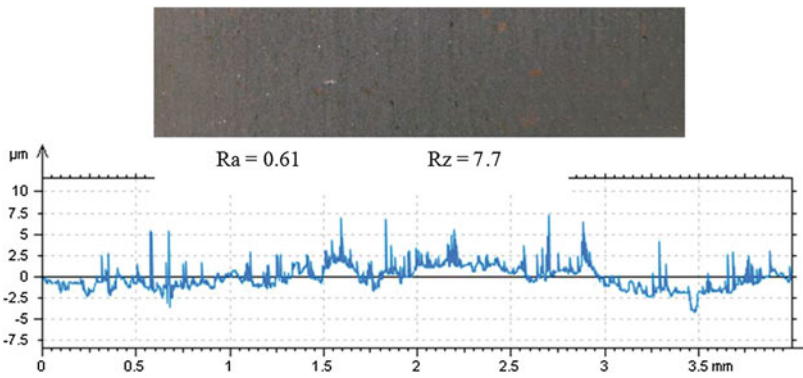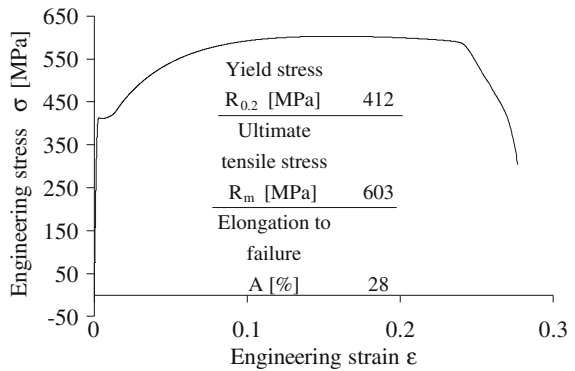**Fig. 30** Stress–strain relationship for C45 steel strip

Fig. 31 Picture of surface and profile roughness parameters for C45 steel sheet (R_a and R_z in μm)

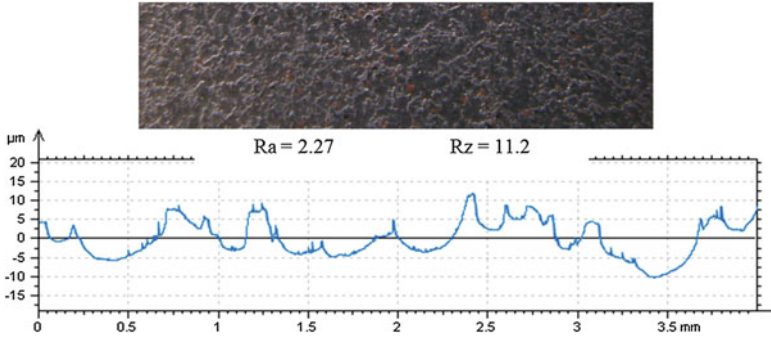**Fig. 32** Stress–strain relationship for 30CrMnSi steel strip

Fig. 33 Picture of surface and profile roughness parameters for 30CrMnSi steel sheet (R_a and R_z in μm)
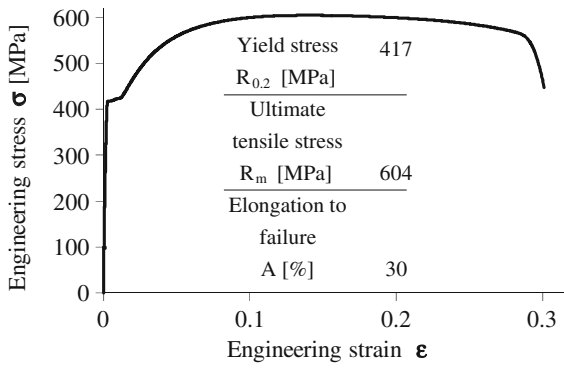

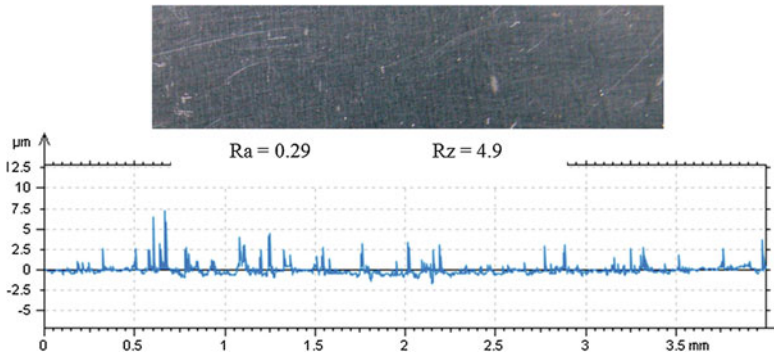**Fig. 34** Stress–strain relationship for 50CrV4 steel strip

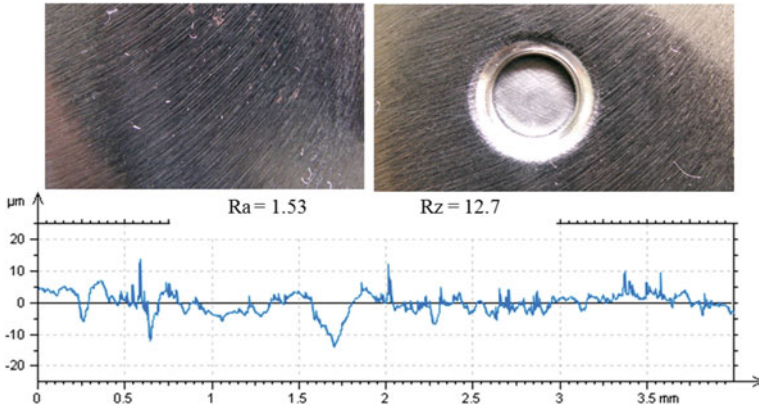**Fig. 35** Picture of surface and profile roughness parameters for 50CrV4 steel sheet (R_a and R_z in μm)

Fig. 36 Picture of surface and profile roughness parameters for C45 steel sheet after grinding (R_a and R_z in μm)
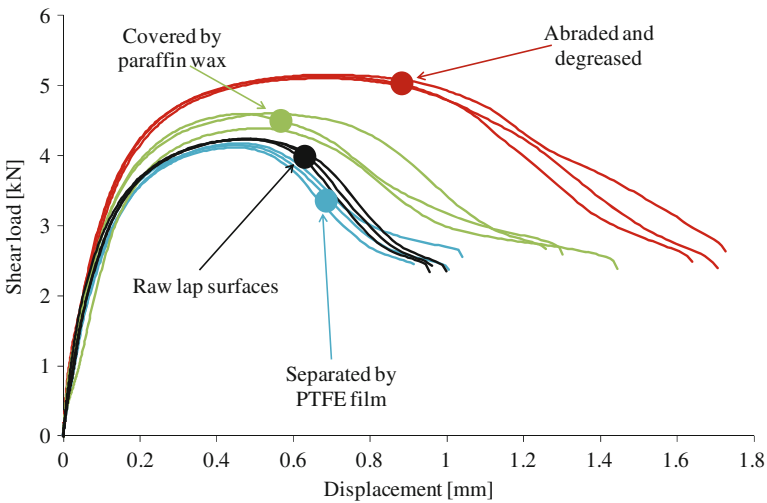

Fig. 37 Experimental load–displacement curves obtained for C45 steel strips clinch joint

C45 specimens with lap surfaces covered by paraffin wax is medium. Another result was obtained for 50CrV4 steel clinch joints (Fig. 39). The greatest shear strength was recorded for the joint when lap surfaces were covered by paraffin wax and medium for the lap surfaces cleaned. This tendency was the same like obtained for the steel–copper clinch joint.

Many repetitions of the shear tests for these materials (C45 and 50CrV4) were done to explain these correlation but it was not unequivocally decided what is the reason of such result. As it could be noticed these materials differ with mechanical
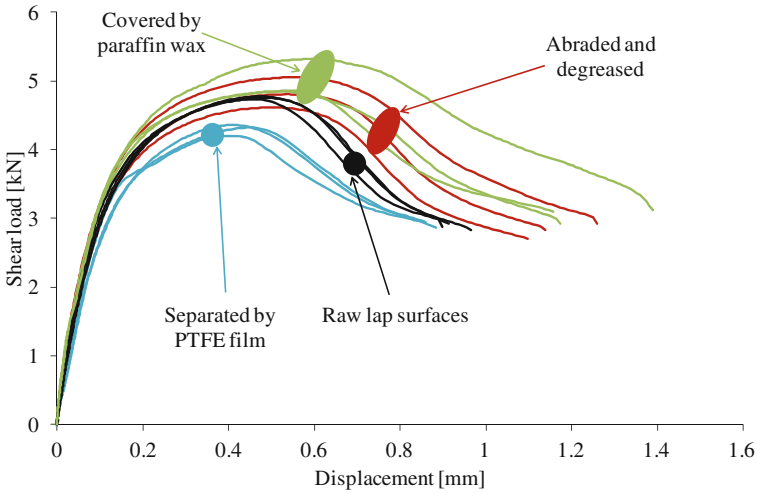
Fig. 38 Experimental load–displacement curves obtained for 30CrMnSi steel strips clinch joint
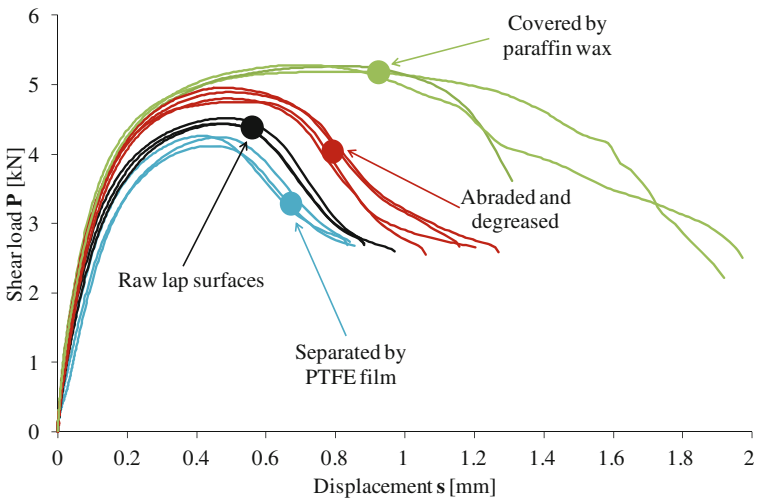
Fig. 39 Experimental load–displacement curves obtained for 50CrV4 steel strips clinch joint

properties and sheet surface roughness. Bigger strength properties for 50CrV4 steel and bigger deformability for C45 steel strips were determined in the tensile test (Figs. 25 and 29). On the other hand the profile roughness parameters of raw sheet materials are better (smaller) for 50CrV4 sheet than for C45 sheet and these parameters determine friction conditions on clinching tools and clinched sheets contact surfaces, what was not tested in the investigations, but it seems to be advantages for the clinch joint decreasing friction on these contact surfaces.

Table 6 Mechanical parameters of structural steels clinch joints

Material	C45		30CrMnSi		50CrV4	
Specimen type	Max. shear load P_{max} (kN)	Energy absorption EA (J)	Max. shear load P_{max} (kN)	Energy absorption (J)	Max. shear load P_{max} (kN)	Energy absorption EA (J)
Lap surfaces covered by paraffin wax	4.5	4.8	5.0	5.1	5.3	7.6
Lap surfaces abraded and degreased	5.1	7.0	4.8	4.5	4.9	4.5
Lap surfaces separated by PTFE film (thickness 0.05 mm)	4.1	3.2	4.3	3.0	4.2	2.8
Raw lap surfaces	4.2	3.3	4.7	3.5	4.5	3.3

Conclusions

The results investigated within this chapter lead to the following major conclusions:

- the clinched joint strength is strongly related to the interface mechanical adhesion between joined sheets, not only to the joint geometrical parameters and joined material properties,
- the clinch joints manufactured with different sheets interface friction conditions have diversified shear strength properties; the load–displacement response is the weakest for joints when lap surfaces are separated by PTFE film, even though compare to joints with raw lap surfaces, without any modification,
- the grinding and degreasing the joint lap surfaces increases the joint strength when compare to the strength of the joint manufactured with raw lap surfaces,
- applying paraffin wax in the clinch joint interface can increase the joint strength in case of some materials (e.g. Cu-ETP—DC4 steel joint and 50CrV4 steel joint) and decrease in case of others (e.g. C45 steel joint), when compare to the joint with grinded and degreased lap surfaces,
- the influence of friction conditions in the tool—sheet contact surfaces and their relationship to the interface friction conditions and the mechanical properties of joined materials should be taken into account to complex estimation of the clinch joint strength.

Adhesive Bonding and Adhesive Type Bonding Joints

Adhesive bonding is a cheap, fast and robust joining technique, widely used in many industrial applications. There are a number of advantages in application of adhesive bonding, e.g. [14–26]:

- this technique does not distort the components being joined as arc-welding has been shown to do,
- better joint stiffness compared to mechanical fasteners or spot-welds because it produces a continuous bond rather than a localized point contact,
- uniform stress distribution over a larger area,
- good energy absorption, damping noise and vibration,
- possibility to join dissimilar, and otherwise incompatible materials.

The main limitations of adhesive bonding are:

- the technology requires heat curing (when thermosetting adhesive is used),
- relatively weak peeling forces,
- sensitiveness to ageing process,
- limited strength under thermal loading.

The most important problem in adhesive bonding is to design the perfect adhesion between joined structural parts. The adhesion at joined surfaces is very complex process, which depends on the type of applied adhesive (composition of the adhesive) and technological process used for curing of the joint. It depends on mechanical, chemical and physical compatibilities of joined materials. The adhesion is created by:

- adhesive penetration of the adherends,
- chemical bonds,
- electrostatic forces,
- molecular bonding,
- moisture-aided diffusion, etc.

All above mechanisms can improve the strength of the interface between adhesive and the adherend, which is particularly very important in the most efforted places of the structural joints, i.e. the ends of the overlap region in joints.

The important limitation of adhesive bonding is the sensitivity of joint strength to pre-treatment which is necessary not only to remove contaminants such as lubricants and oils, but also to provide the intimate contact needed for the adhesive to bond successfully with the adherend surface.

The safe design of high-speed commercial airplanes requires in designing process to take into account the operational temperature level (OTL). The behaviour of the adhesives in different temperature results from their polymetric nature and is related to so called glass transition temperature (GTT). It depends on the chemical composition of the adhesive and molecular interaction as well as degree of cross-linking resin. Moreover, the higher curing temperature of the adhesive leads to increase of the GTT. Therefore, in designing of any structural joint the level of operation temperature should be much below the GTT of the adhesive and the hot curing adhesive should by applied for structural elements subjected to high OTL.

Aging problems of the adhesive layers are very substantial for durability and reliability of the structural elements. The most important issues are:

- moisture exposition, i.e. water absorption or desorption,
- high or low level of temperature,
- corrosive environment (e.g. salt spray, chemical agents, etc.).

All of these negative factors can lead to degradation of the mechanical and physical adhesive properties (e.g. cohesive strength, embrittlement, shrinkage) as well as degradation of the adhesion properties at the interface of joined materials. Therefore, it is necessary to perform appropriate surface preparation of joined adherends to decrease the risk of quick corrosion degradation of the joints.

However, the adhesive bonding can be used as a supporting technique to increase the strength of mechanical joints and to make them watertight. In this manner various kinds of so called hybrid joints can be created, see [11–14, 24, 27–33].

The other type of bonding using adhesive forces is adhesive tape bonding applied to creation of hybrid joints (i.e. the clinch-adhesive joint), e.g. [34] and [35]. The authors propose using pressure-sensitive adhesive tape or structural bonding tape. The advantages of this approach include: quick-fix properties of joined components, good viscoelastic properties under impact loading and vibration damping properties. The proposed type of hybrid joints exhibits pressure-sensitive properties from ambient temperatures to 140 °C and can be cured to develop good structural properties. However, until now the used pressure-sensitive adhesive joints are limited by their creep under static mechanical load and relatively low strength at elevated temperatures.

Numerical Model Applied for Modelling of Simple and Hybrid Joints

To complete the analysis of the simple: purely adhesive or clinched joints we briefly discuss details of the FE models necessary to trace deformation process of joints. The first papers with application of the FE methodology deal with description of the forming process [36, 37], but without inclusion of damage in the elasto-plastic material.

The situation becomes more complicated in case of mechanical response estimation of the simple or hybrid joints, due to the fact of complex shape of structural elements. The failure process of joints under quasi-static loading passes through several stages and 2 kinds of different damage mechanisms are activated:

- gradual degradation of the adhesive layer,
- continuous degradation of the elasto-plastic adherends, in particular in clinching points.

According to [12, 14, 24, 31, 32] in order to create the FE model of the simple or hybrid joints 2 kinds of FE were used:

- cohesive elements—for the modelling of the adhesive layer,
- solid elements including plastic damage (ductile damage model—DDM) or porosity nucleation and growth (Gurson-Tvergaard-Needleman model—GNT), which are related to the current level of loading or plastic strains.

Cohesive Zone Model (CZM)

In order to simulate gradual decohesion and the failure process of the adhesive layer, a CZM model was applied in FEA calculations. Figure 40a shows the triangular stress-separation law for the uniaxial case. λ is non-dimensional opening displacement equal to:

$$\lambda = \frac{u_n}{\delta^{\max}} \tag{2}$$

where u_n is the normal opening displacement and $\delta^{\max}$ is a maximum opening displacement. $\sigma^{\max}$ is the maximum stress threshold for the modeled material, whereas λ_{in} corresponds to the non-dimesional displacement indicating damage initiation in the material. Figure 40b presents the trapezoidal rule, particularly suitable for adhesive exhibiting plastic response.

G_{Ic} is the area under the curve corresponding to the absorbed energy to fracture. In 3-D cases, Figs. 12 and 13 (e.g. Needleman [38] and Tvergaard and Hutchinson [39]), where a complex mode of damage growth occurs, it is necessary to introduce a normal opening displacement u_n for the tension mode and a tangential displacement u_τ for the shear mode. Similar to (2) it is possible to define non-dimensional displacements λ_n and λ_τ:

$$\lambda_n = \frac{u_n}{\delta_n^{\max}}, \quad \lambda_\tau = \frac{u_\tau}{\delta_\tau^{\max}}, \tag{2}$$

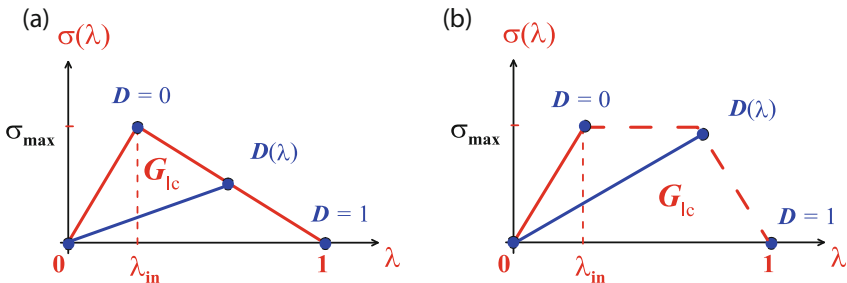**Fig. 40** Stress–displacement rules for CZM with damage parameter D: **a** triangular, **b** trapezoidal

where $\delta_n^{\max}$, $\delta_\tau^{\max}$ are the maximum opening and shear displacements. We assume for the considered 3-D case that the damage initiation criterion will depend on current state of stress $\{\sigma_n, \sigma_t, \sigma_s\}$ and is expressed by:

$$\left(\frac{\sigma_n}{\sigma_n^{\max}}\right)^2 + \left(\frac{\sigma_t}{\sigma_t^{\max}}\right)^2 + \left(\frac{\sigma_s}{\sigma_s^{\max}}\right)^2 = 1, \tag{3}$$

where σ_n is the normal stress to the surface of the adhesive layer, whereas σ_t and σ_s are the shear stress components along the adhesive layer. The values of $\sigma_n^{\max}, \sigma_t^{\max}, \sigma_s^{\max}$ are the threshold values of the stress state corresponding to initiation of damage process described by parameter $D(\lambda)$ for the uniaxial case (Fig. 40) or $D(\lambda_n, \lambda_t, \lambda_\tau)$ in the general 3-D case:

$$D(\lambda_n, \lambda_t, \lambda_\tau) = \sqrt{(\lambda_n)^2 + (\lambda_t)^2 + (\lambda_\tau)^2} \tag{4}$$

The failure criterion in the most general case is formulated as a power law and depends on the fracture energy in the three considered modes: normal $n = I$ and two tangential: $t = II$, $s = III$:

$$\left(\frac{G_I}{G_{Ic}}\right)^2 + \left(\frac{G_{II}}{G_{IIc}}\right)^2 + \left(\frac{G_{III}}{G_{IIIc}}\right)^2 = 1 \tag{5}$$

where G_{Ic}, G_{IIc}, G_{IIIc} are the critical values of the fracture energies (CFE). In case of lack of all above values of CFE estimated experimentally, one can assume that $G_{IIc} = G_{IIIc} = G_{Ic}$, i.e. the failure of the cohesive layer is isotropic.

Gurson-Tvergaard-Needleman (GTN) Damage Model for Ductile Material

The damage development in the metallic parts of the joints can be estimated with application of the GTN model, e.g. [24, 31, 40]. The modelled material is assumed to be plastically isotropic with inclusion of homogeneously distributed porosity, which is given as a void volume fraction f, i.e. as a ratio of the volume of porosity to the total volume of the material.

The yield condition is defined by the plastic potential F:

$$F\left(\sigma_{eq}, \sigma_m, \bar{f}, q_1, q_2, q_3, \sigma_y\right) = \left(\frac{\sigma_{eq}}{\sigma_y}\right)^2 + 2q_1\bar{f}\cosh\left(1.5\,q_2\frac{\sigma_m}{\sigma_y}\right) - 1 - (q_3\bar{f})^2 = 0 \tag{6}$$

where σ_{eq} is the Huber–von Mises equivalent stress, σ_m is the hydrostatic component of the stress state, σ_y is the yield stress. q_1, q_2, q_3 are 3 coefficients of the model.

$$\bar{f} = \begin{cases} f & \text{for } f \leq f_c, \\ f_c + \delta(f - f_c) & \text{for } f > f_c \end{cases}, \tag{7}$$

where f_c is the critical porosity at the onset of void coalescence. The GTN model allows for taking into account the porosity nucleation and growth by the rate equation:

$$\dot{f} = \dot{f}_{\text{nucl}} + \dot{f}_{\text{growth}} \tag{8}$$

Ductile Damage Model DDM for Plastic Materials

The basis for this ductile phenomenological model is the observation of initiation, growth and further coalescence of the voids [41, 42]. Figure 41 presents the whole stress-strain diagram for the DDM. The damage process begins at the peak of this constitutive curve and up to this moment the Young's modulus of the material has a constant value ($E = $ const.). The onset of damage in the model takes place for the equivalent plastic strain $\bar{\varepsilon}_{eq}^{\text{pl}} = \bar{\varepsilon}_0^{\text{pl}}$:

$$\bar{\varepsilon}_0^{\text{pl}} = \bar{\varepsilon}_0^{\text{pl}}(\eta, \dot{\bar{\varepsilon}}_0^{\text{pl}}), \tag{9}$$

which is a function of stress triaxiality $\eta = \sigma_m/\sigma_{eq}$ and the equivalent plastic strain

Fig. 41 Ductile Damage Model (DDM) for the elasto-plastic material
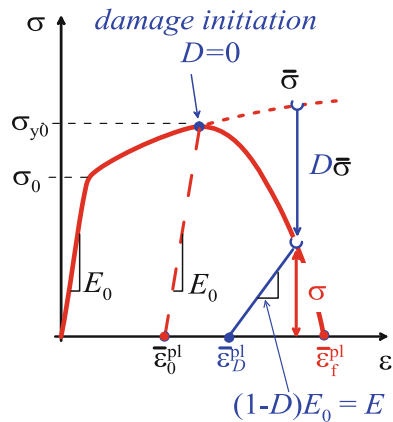
rate $\dot{\bar{\varepsilon}}_0^{pl}$. Damage process starts when the following criterion is satisfied:

$$\omega_D = \int \frac{d\bar{\varepsilon}^{pl}}{\bar{\varepsilon}_0^{pl}(\eta, \dot{\bar{\varepsilon}}_0^{pl})} = 1, \tag{10}$$

where ω_D is a state variable that increases monotonically with the plastic deforma-
tions. Then for $\bar{\varepsilon}_{eq}^{pl} > \bar{\varepsilon}_0^{pl}$ damage develops, i.e. the variable D increases from 0 to the
final value 1, $(D \in (0 \rightarrow 1))$ and the current state of stress is equal to (e.g. [43–47]):

$$\sigma = (1 - D)\bar{\sigma} \tag{11}$$

where $\bar{\sigma}$ is the effective (undamaged) stress tensor. It can be seen in Fig. 7 that the
$D\bar{\sigma}$ denotes the loss of the loading capacity of the material by the current damage
state described by the variable D. One can notice that damage of the material causes
a decrease of the initial Young's modulus E_0, i.e. the material unloading is
described by the current value of the elastic unloading modulus:

$$E = (1 - D)E_0 \tag{12}$$

The material loses its load carrying capacity for the equivalent plastic strain $\bar{\varepsilon}_{eq}^{pl} = \bar{\varepsilon}_f^{pl}$ when the damage variable reaches the final value $D = 1$.
In order to describe the material's behaviour numerically after damage initiation,
the fracture energy approach [41] was applied by the introduction of the material
parameter—G_I—energy required to open a unit area of crack, creating a stress-
displacement response. The implementation of this concept in a FEM model was
necessary in order to introduce a characteristic length, L, associated with the
integration point. Then the fracture energy is given by:

$$G_I = \int_{\bar{\varepsilon}_0^{pl}}^{\bar{\varepsilon}_f^{pl}} L\sigma_y \, d\bar{\varepsilon}^{pl} = \int_0^{\bar{u}_f^{pl}} \sigma_y \, d\bar{u}^{pl}, \tag{13}$$

where $\bar{u}^{pl}$ is the equivalent plastic displacement, which can be defined as the
fracture energy conjugate of the yield stress after damage initiation, and is equal to:

$$\dot{\bar{u}}^{pl} = L\dot{\bar{\varepsilon}}^{pl}, \tag{14}$$

The damage evolution law can be specified in terms of the equivalent plastic
displacement $\bar{u}^{pl}$, or in terms of the fracture energy dissipation G_I. Both of these
options take into account the characteristic length of the element to alleviate mesh
dependency of the results. The damage governing equation can be expressed as the
equivalent plastic displacement $\bar{u}^{pl}$:

$$D = D(\bar{u}^{\mathrm{pl}}) \tag{15}$$

In general, we have linear, piecewise linear or exponential form of (15).

Numerical FE Model of Simple and Hybrid Joints

The analysed joints were numerically modelled with application of the ABAQUS commercial code ver. 6.14. In calculations due to large plastic deformation we used Lagrangian-Eulerian adaptive meshing and the explicit solver with the stability time increment, less than the stability limit.

The damage processes were modelled:

- in adhesive layers by application of the CZM,
- in metallic adherends by using DDM.

The created model was effectively used to calculate deep drawing process of the joint during clinching as well as to modelling deformation of the joints.

Clinch-Adhesive Joints

Increase of clinch joints can be done by additional bonding of joined components. This solution seems to be very beneficial—applying two different joining techniques causes accumulation of their advantages and elimination of their defects.

Adhesive bonding is a cheap, fast and robust joining technique, widely used in many industry applications. There are a number of advantages applying adhesive bonding, described in section "Adhesive Bonding and Adhesive Type Bonding Joints". The most important feature of the adhesive bonding is that it can be used as a supporting technique to increase the strength of mechanical joints and to make them watertight.

The adhesive bonding process can be combined with resistance spot welding, riveting or mechanical fasteners in hybrids joints [27–33]. This hybrid process of joining is used to maximize the benefits of the various joining processes [20, 48, 49].

The advantage of the clinch-adhesive joining is that it allows the use of not only fluid and pasty adhesives, but also of adhesive foils and bands, Fig. 42. Clinching without local incision can be used with pasty adhesives, whereas the application of an adhesive foil or band is more appropriate when small incisions are created during the manufacturing process.

In comparison to pure clinching, Fig. 3, one can notice that in hybrid fastening an additional strengthening mechanism of the joint is created by the adhesive in the clinching place and also in the overlapping area of the hybrid joint, Fig. 43. It significantly increases the load capacity of the joint and its energy absorption during failure.
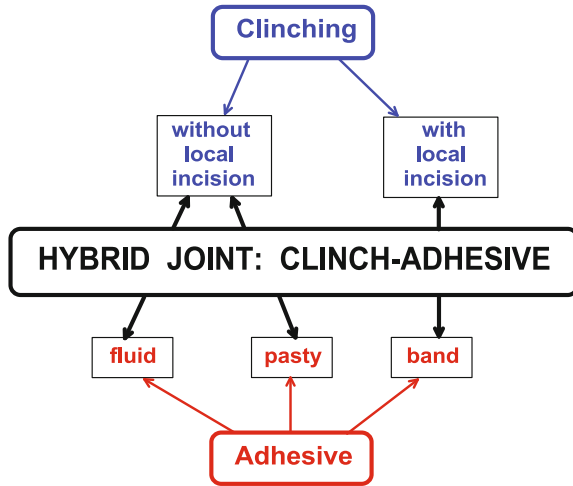
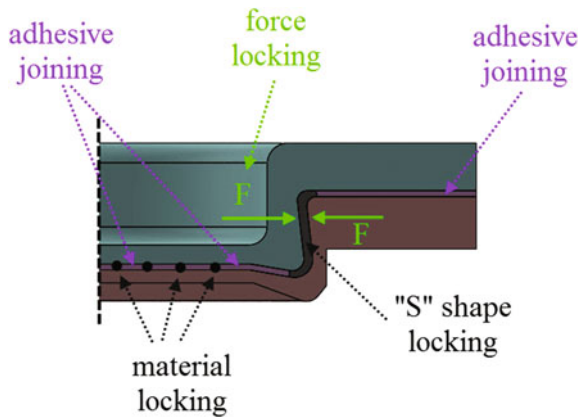**Fig. 42** Manufacturing of clinch-adhesive joints

Fig. 43 Mechanisms of clinch-adhesive joining

When the area of the punch (cross section) is much higher than 70 % of the area of the die, a certain part of the side surface of the clinch contains local incisions, Fig. 44. This causes the global weakening of the connection of the fastened materials due to material discontinuities, which create local stress concentrations. This technology cannot therefore be recommended for automotive and aeronautical structural applications.
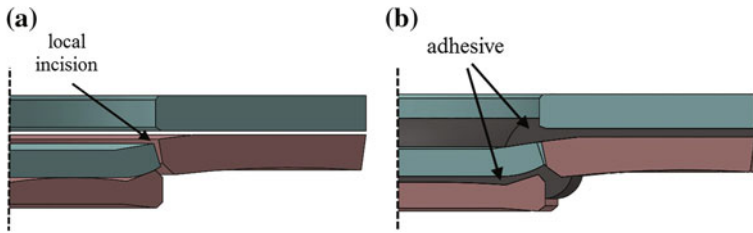
Fig. 44 Clinch joints with local incision: **a** pure clinching, **b** clinch-adhesive joint

Experimental Program—Shear and Peel Tests on Single and Hybrid Lap Joints

The range of experimental investigations, presented here, included shear tests on single lap joints. The aim of experiments was increasing the shear strength of clinch joints. Single lap joints were manufactured and tested as clinched, adhesively bonded, and hybrid: clinched–adhesively bonded, Fig. 45. The clinch-adhesive hybrid joints were made with application different kinds of commercial adhesives. Three sheet materials were used in this study: ETP-copper, CuZn37 brass, and low-carbon steel. The thickness of all sheets was about 1 mm. Pure aluminium sheets were not used in this tests because the hybrid joint strength was greater than the sheet strip strength and hybrid specimens were destroyed by sheet ductile fracture instead of shear the joint as shown in Fig. 46.

Application of the 2-Component Strong Brittle Epoxy DRAGON

The adhesive used in the first series of experiments was Dragon® (Chemical Factory DRAGON, Cracow, Poland), a two-component brittle epoxy for metal joining. The curing cycle of the adhesive was 4 h at 20 °C and then it was accelerated by heating. The full strength of the joint was obtained after 24 h. This adhesive is used to join different combinations of materials, such as steel, cast iron, aluminium, metal alloys, ceramics and plastics.

Adhesively bonded joints were manufactured with an overlap of 35 mm (Fig. 45). The procedure for the hybrid joint specimen preparation was the following (Fig. 47):

- cleaning of the joined parts (abrasive paper and acetone),
- adhesive application and pressure,
- curing process for 24 h at room temperature,
- clinching.

The average thickness of the adhesive layer was about 0.15 mm.
The strength characteristics of hybrid joints compared with those of clinched joints are shown in Figs. 48, 49, 50, 51, 52 and 53. The adhesive joint curve of brass
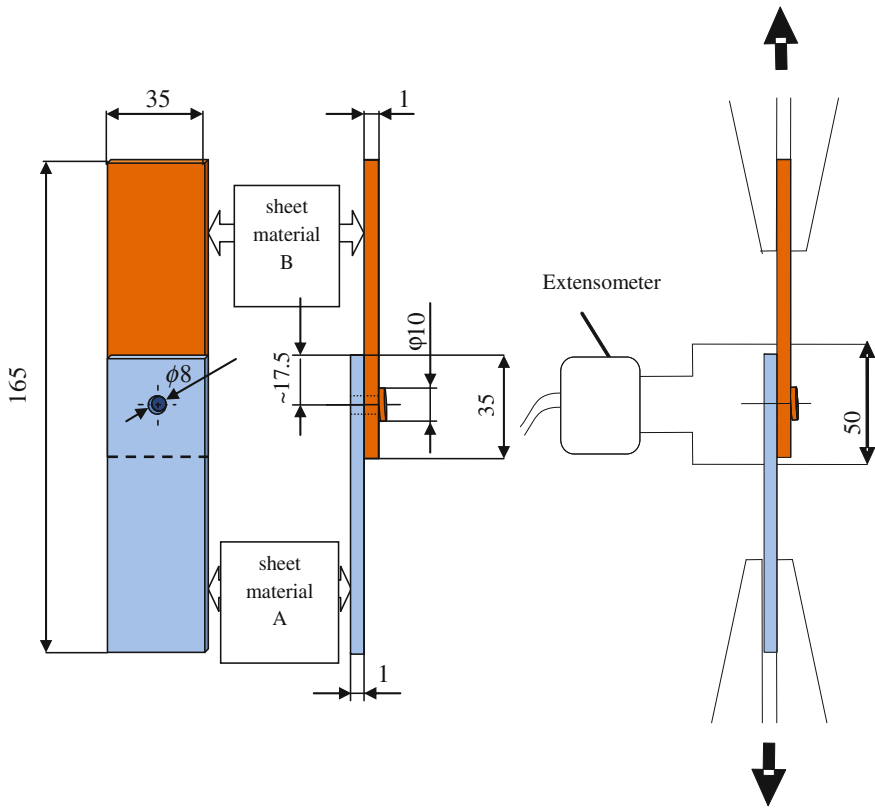
Fig. 45 Geometry of overlap clinch joint specimen and the shear test arrangement

sheets is shown in Fig. 48. The clinched joint of brass–brass sheets is very weak and it does not influence significantly the hybrid joint strength characteristics (load–displacement curves of hybrid and adhesive joints are comparable).

When materials create strong clinched joints, i.e., steel–steel, steel–copper and copper-steel, applying adhesive enhances its strength but total hybrid joint strength is not high value (in comparison with the adhesive joint). The strength characteristics of these materials have a special feature—when the adhesive fails, the clinch still keeps the materials connected which results in high elongation (Figs. 50, 52 and 53) and energy absorption (Table 8). The strong clinched joints are formed by high deformation of joined sheets, but it results in greater area of destroyed adhesive layer and diminishing of total strength of hybrid specimen. When the strength of the clinched joint is low, the strength of the hybrid joint is high (Figs. 48, 49 and 51) and clinched joint failure is not so distinct in strength characteristic (in case of brass–brass joint, it is not visible at all).

The increase of clinched joint strength caused by additional applying adhesive (i.e. in hybrid joint) is considerable. As it can be seen in Figs. 50, 52 and 53, it is

Fig. 46 Hybrid clinch-adhesive joint of aluminium sheets after pull test
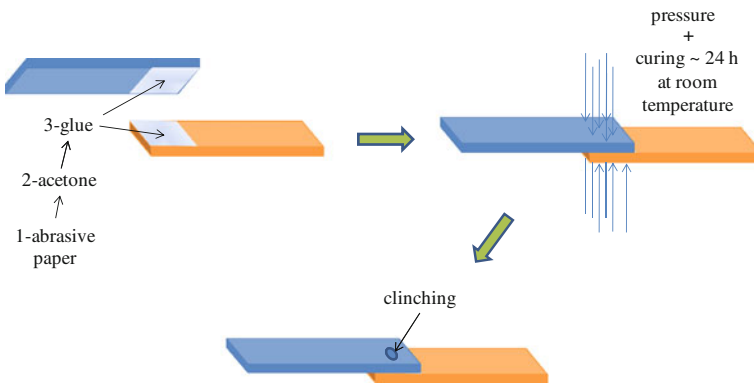

Fig. 47 Methodology of hybrid specimen—curing of adhesive before clinching

about 40 % for steel-steel joint, 70 % for steel–copper joint and till 83 % for copper–steel joint.

The clinched joint parameters (Fig. 6): *x*, *th* and *cl* as well as a longitudinal cross-sectional view of the hybrid single lap joints are shown in Table 7. It can be seen that the joint parameters are related to clinched joints strength. The lowest
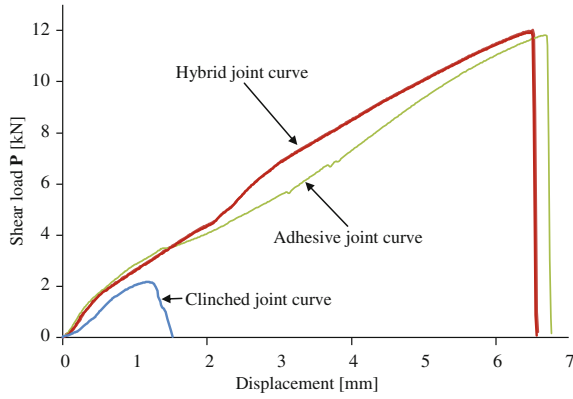
Fig. 48 Experimental load-displacement curves (clinch, adhesive and hybrid) obtained for brass–brass joint
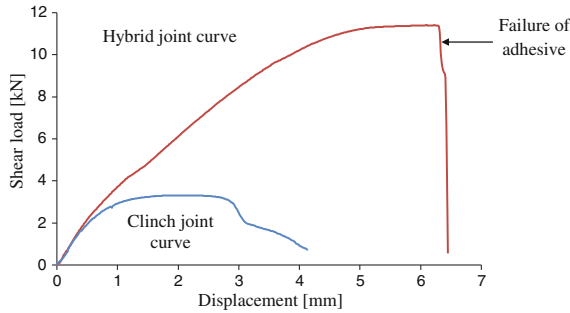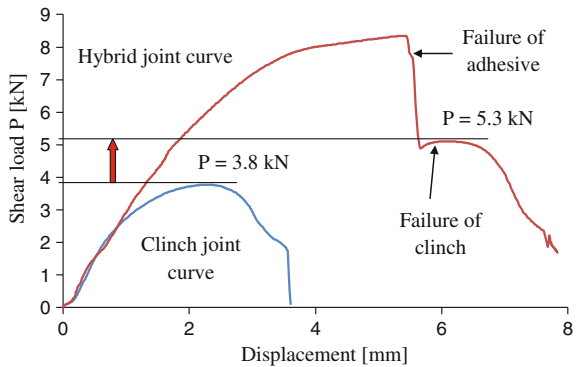

Fig. 49 Experimental load–displacement curves (for clinched and hybrid joints) obtained for copper–copper joints

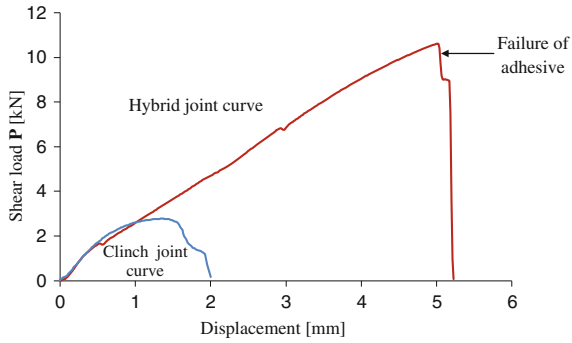**Fig. 50** Experimental load–displacement curves (for clinched and hybrid joints) obtained for steel–steel joints

Fig. 51 Experimental load–displacement curves (for clinched and hybrid joints) obtained for brass–copper joints
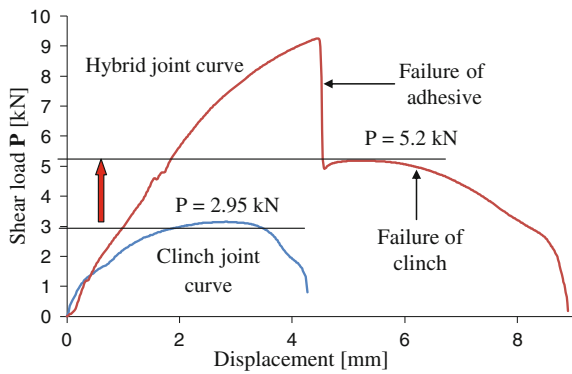

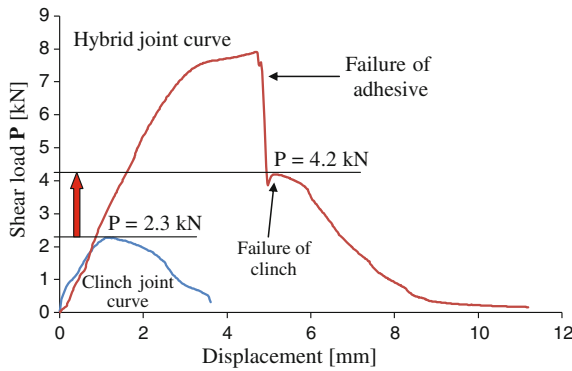**Fig. 52** Experimental load–displacement curves (for clinched and hybrid joints) obtained for steel–copper joints

Fig. 53 Experimental load–displacement curves (for clinched and hybrid joints) obtained for copper–steel joints
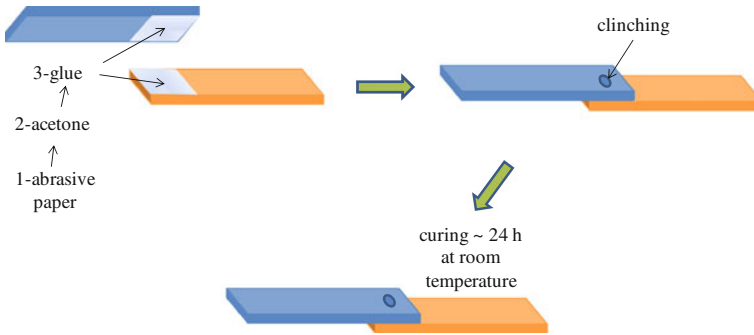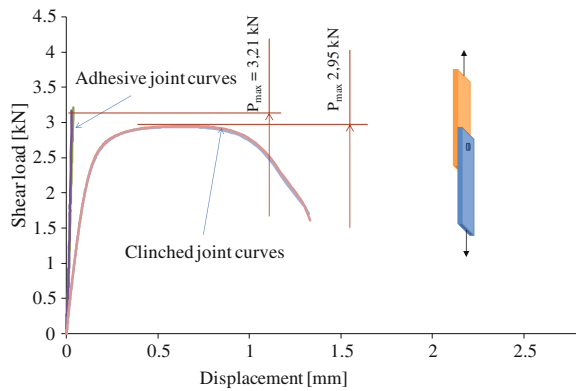
Fig. 54 Methodology of hybrid specimen—linching before curing of adhesive

Fig. 55 Shear load–displacement curves obtained in pull test for adhesive and clinch joints

closure was measured for steel–brass joint, and the biggest for steel–copper joint. In case of joints with copper, folding is visible in the bottom corner of the joint cavity, i.e. the adhesive caused a buckling of the lower material in the die groove. The same phenomena was observed when thick PTFE film was applied in the lap interface (Fig. 15d). There is no difference in the shape of the upper material deformed by the punch; it is comparable with the one in the clinched joint without adhesive.

Table 8 gives of the energy absorption (EA) of all considered types of joints. Adding the adhesive into the clinched lap joint significantly increases the strength of the joint. The adhesive joint starts to fail at the maximum shear force, so the hybrid joint energy absorption was divided into two parts: before and after the maximum shear force. This allowed to estimate that when the clinched joint was strong, EA after the maximum shear force was high (but lower than the one before this maximum).With the application of the adhesive, the EA of hybrid joints manufactured from steel or steel–copper increases about 4.5 times in relation to pure clinching. It is interesting to notice that this increase up to the maximum peak of the force–displacement diagram is equal to 2.5–3 times. In the case of the

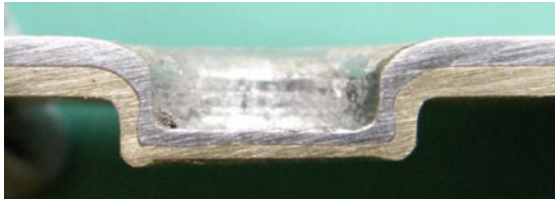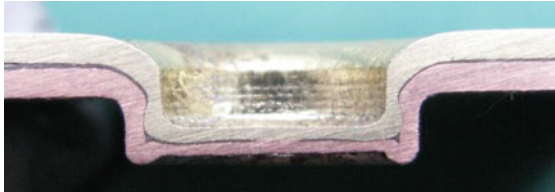**Table 7** Clinched joint parameters in hybrid lap joints

Joined materials	Thickness of the clinched bottom x (mm)	Min. thickness of the upper sheet th (mm)	Interlock cl (mm)
Steel–brass	1.0	0.51	0.15
Brass–copper	0.96	0.45	0.18
Steel–copper	0.94	0.5	0.19

Table 8 Energy absorption of clinch and hybrid joints

Joined materials	Energy absorption (J)			
	Clinch joint	Hybrid joint		
		Before max. shear force	After max. shear force	Total
Steel–copper	10.4	24.9	19.3	44.2
Steel–steel	9.6	31.5	10.5	42.1
Copper–copper	9.9	46.9	3.7	50.6
Brass–copper	3.7	28.9	1.9	30.8
Brass–brass	1.9	44.0	0.4	44.5

copper–copper, brass–copper and brass–brass joints, almost the whole energy accumulation takes place up to the force maximum. The addition of the adhesive to the copper–copper joint is the most effective way to increase EA. Pure clinch joints made of brass and brass–copper are very weak when it comes to EA accumulation. Introduction of the adhesive layer diametrically changes the mechanical performance of these joints. It is particularly visible in the case of the brass–brass joints, where the increase of EA is approximately 20 times. To conclude the analysis of the EA parameter for the joints efficiency, one can state that the most effective application of the adhesive is in the case of the copper–copper and brass–brass joints.

Application of the Weaker Glue Pattex® Repair Epoxy

The tests of hybrid clinch-adhesive joints were continued with applying another commercial glue Pattex® Repair Epoxy. In above presented shear tests the adhesive and hybrid specimens bonds in lap area were bigger then tensile yield point of sheet metals. To avoid this effect the weaker glue was applied, i.e. Pattex® Repair Epoxy a commercial product of Henkel AG & Co. KGaA. Manufacturer defined properties for this adhesive were: drying time—5 min, allowable move time—15 min, curing time—2 h, adhesive strength—12 MPa. ETP-copper and low carbon steel were used as the sheet materials.

Two methodologies of hybrid specimen were applied: (1) adhesive curing before clinching (as it was used with adhesive Dragon® and the procedure is shown in Fig. 47) and (2) clinching before adhesive curing (procedure is shown in Fig. 54). Because of short time of allowable drying and moving time, clinching in the 2-nd procedure was made directly after adhesive spread.

The range of experimental investigations included the pull (specimen geometry is shown in Fig. 45) and peel (specimen geometry shown in Fig. 58) tests of single lap joints.

Mechanical characteristics of base joints (i.e. clinch and adhesive joints) recorded during pull test are shown in Fig. 55. Applying Pattex® caused that the maximal shear loads for adhesive and clinch joints are comparable each other (3.21 and 2.95 kN respectively). Linear characteristic of adhesive joint means that sheet yielding point was not obtained (what occured when applying adhesive Dragon®).

Mechanical characteristic of hybrid joint prepared by procedure clinching after curing is shown in Fig. 56. The maximal shear load is much higher than maximal shear loads of component joints, what can be explained by synergy effect. When adhesive joint failures, the shear load falls and the joined sheets are still kept together by clinch joint. The part of load–displacement curve after maximal shear load point is mechanical characteristic of the clinch joint enhanced by adhesive. It can be seen 22 % growth of maximal load obtained for the pure clinch joint strength. The growth is evident in total displacement recorded by extensometer, too (about 1.6 times longer for clinch joint in hybrid connection).

Much greater synergy effect was recorded in the pull test for hybrid joint prepared by procedure 'clinching before adhesive curing' (Fig. 57). Maximal shear
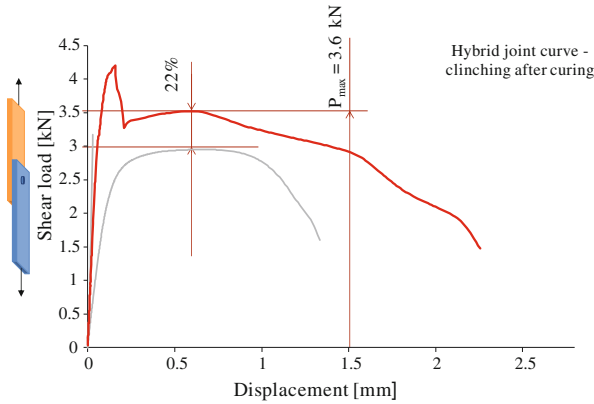
Fig. 56 Shear load–displacement curves obtained in the pull test for clinching after curing hybrid joint
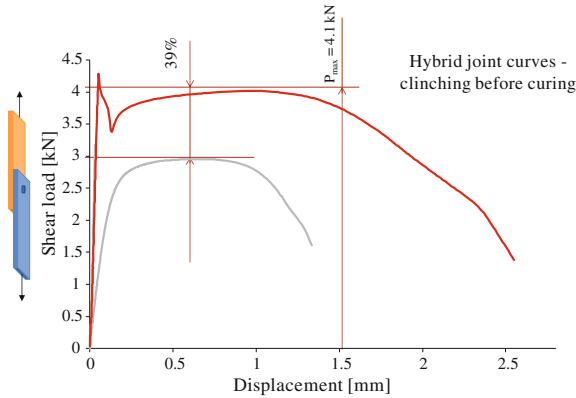

Fig. 57 Shear load–displacement curves obtained in the pull test for clinching before curing hybrid joint

load of the clinch joint stage of the pull test characteristic is almost comparable with the maximal shear load of the hybrid joint and is about 39 % greater than one obtained for the pure clinch joint.

The shape and overall dimensions of specimens used in peel test are shown in Fig. 58. The T shape specimens were used and three clinched point joints were applied in case of the clinch and hybrid specimens. For each specimen the results of the maximal peel load and energy absorption were averaged form three peak values.

The results of the peel test obtained for the pure adhesive and the pure clinch joints are shown in Figs. 59 and 60 respectively. Generally it can be reported that the peel strength of tested joints is much lower than the pull one. Additionally the peel test of pure adhesive joints show relatively big spread of recorded
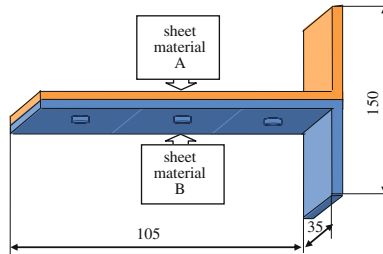
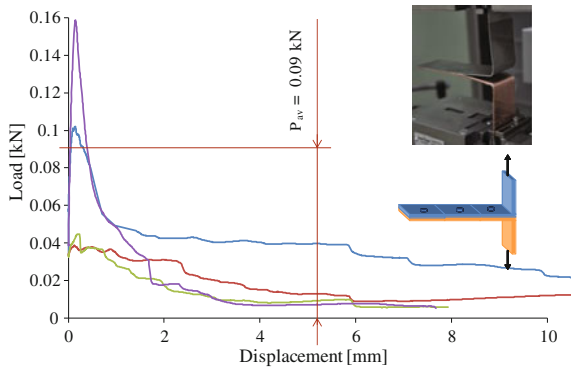**Fig. 58** Geometry of peel test specimen (A–B joint materials)

Fig. 59 Peel test curves obtained for adhesive joint

load–displacement curves (Fig. 59). The greater values of the averaged maximal peel load were recorded for the pure clinch joint than the pure adhesive joint, what is the inverse result of the pull test.

The results of the peel test for two procedures of the hybrid specimen are shown in Figs. 61 and 62. The peel test curves, for both kind of hybrid specimen preparation procedure, have the same character like clinch joint specimen; there are three peak values of peel load and the first peak value is the lowest. As it was in the pull test the procedure 'clinching before adhesive curing' gives better results of the joint strength than the procedure 'clinching after adhesive curing'.

The summary of results obtained in the tests with applying Pattex® Repair Epoxy are shown in Table 9. The hybrid joint strength is the pull test is strongly influenced by adhesive joint properties; opposite relation can be reported in the peel test when the hybrid joint strength is mainly determined by clinch joint character. Greater values of energy absorption were recorded in the peel tests for clinch and hybrid joints and this is the result of plastic deformation (bending) of sheet strips during the test.
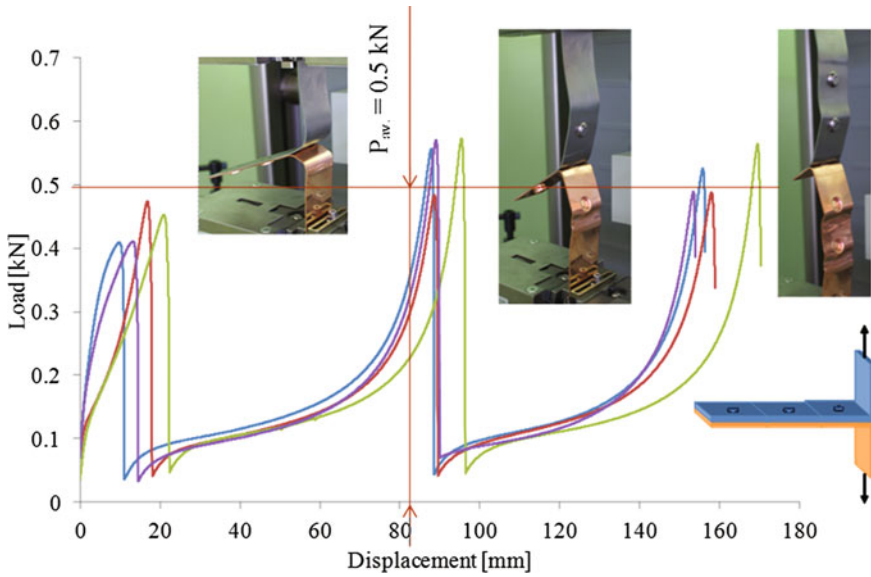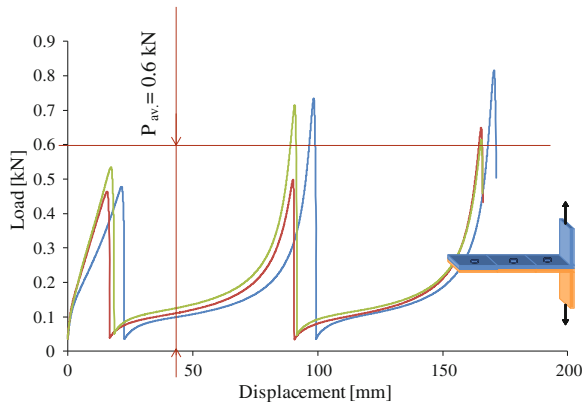
Fig. 60 Peel test curves obtained for clinch joint

Fig. 61 Peel test curves obtained for hybrid joint (adhesive curing before clinching)

Application of the Flexible Adhesive (Adhesive Type Bonding)

Hybrid clinch-adhesive joints can be made by applying flexible adhesives, too. Flexible adhesives are characterized by low elastic modulus and high extensions to failure. These adhesives are mostly used when considerable expansion and contraction is expected in the joint, when flexibility of the joint is required or good gasket or sealing properties are necessary; they also properly resist impact and vibration [25].

Fig. 62 Peel test curves obtained for hybrid joint (clinching before adhesive curing)
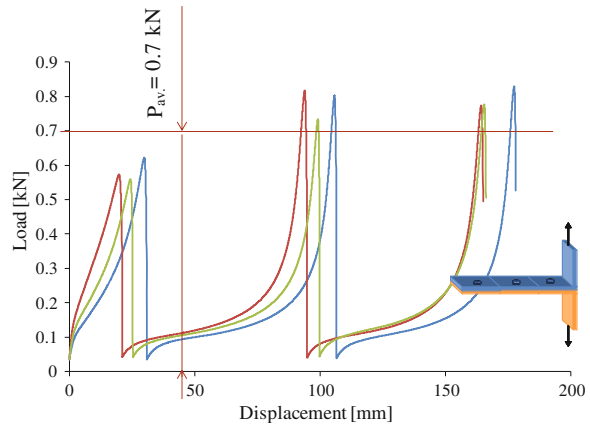

Table 9 Mechanical parameters of the steel–copper joints determined in the pull and peel tests (averaged values for one joint point)

Type of joint	Maximal load P (kN)	Energy absorption EA (J)		Maximal load P (kN)	Energy absorption EA (J)	
Adhesive	3.21	0.06		0.09	0.02	
Clinch	2.95	3.3		0.5	7.1	
Hybrid—clinching after adhesive curing	4.25	6.6		0.6	10.7	
Hybrid—clinching before adhesive curing	4.31	8.6		0.7	11.6	

Hybrid joints made with applying flexible adhesives are shown in Figs. 63 and 64. The adhesives chosen to the tests were: chlorinated rubber and double faced polypropylene (PP) tape thickness ~ 0.2 mm. The effect of clinch strength increasing was not obtained; the shear curves of clinch and hybrid joints are comparable.

Applying elastic adhesive is not advantageous for the clinching process; it makes difficulties during clinching and an appropriate interlocking of the clinch joint could not be obtained (low values of cl parameter). In case of PP tape, the characteristic sheet bending at the die groove occurred, like when applying thick PTFE film.
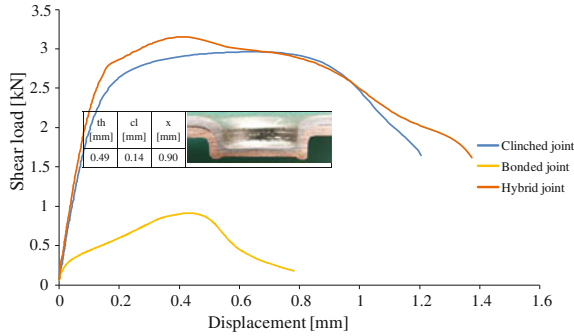
Fig. 63 Pull test characteristics and geometrical parameters of steel–copper lap joints (chlorinated rubber used as the adhesive agent)
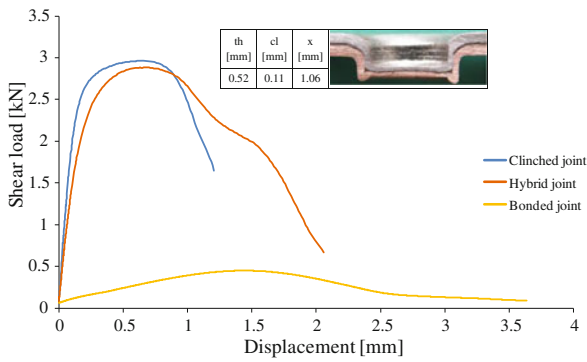

Fig. 64 Pull test characteristics and geometrical parameters of steel–copper lap joints (double faced PP tape used as the adhesive agent)

Conclusions

This part of the experimental program can be concluded in the following way:

- the strength of clinch-adhesive hybrid joints strongly depends on both the adhesive and adherends properties. Application of a brittle and stiff adhesive leads to progressive damage and failure in the adhesive layer during finite plastic deformations. The strength of hybrid joints are 3–6 times higher in comparison to purely clinched joints,
- a two-stage fracture process (first in the adhesive and then in clinching) in the considered hybrid joint significantly increases the energy absorption up to final failure in comparison to pure clinched joints.
- taking into account the wide range of different types of joined materials and commercial adhesives available (from stiff and strong to flexible and ductile),

elaboration of the proper joining technique should include the choice of appropriate values of the parameters *cl*, th and *x* as well as adhesive.

Numerical Modelling of the Hybrid Joints Mechanical Response

Modelling of Deep Drawing Process

The FEA investigations concerned the clinched joint and the clinch-adhesive hybrid joint of low carbon steel and copper sheets. The three dimensional (3-D) model used in the FEA simulations consisted of (Fig. 65):

- two joined sheets,
- the adhesive layer,
- the punch,
- the blank holder,
- the die.

Because of the axisymmetric structure of the clinched joint, only half of the joint was modeled. The forming tools: the punch, the blank holder and the die were assumed as undeformable rigid bodies. The dynamic explicit FEA simulation included the following steps:

- Drawing—punch displacement: 3.8 mm in 0.001 s,
- tools reverse—punch and die displacement of the specimen surface: 8 mm in
- 0.0001 s,
- specimen failure under shear deformation process of specimen: distance 10 mm in 0.001 s.

During the FEA simulation, arbitrary Lagrangian–Eulerian adaptive meshing was used in order to obtain good quality of the finite element mesh under large plastic deformation. Friction formulation type penalty was assumed with friction coefficients between sheets of $\mu = 0.3$ and between sheets and tools of $\mu = 0.1$. The
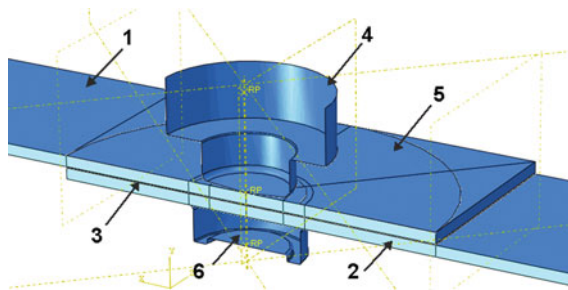

Fig. 65 Elements of numerical model of hybrid clinch-adhesive forming process: *1* upper steel sheet, *2* lower copper sheet, *3* adhesive layer, *4* punch, *5* blank holder

3-D FEA model consisted of 34,480 elements, including one sheet model with eight node elements (4 elements in thickness), the adhesive layer with eight node cohesive elements (1 element in thickness), the punch, the blank holder and the die with four node 3-D rigid elements.

The details of deep drawing process were analysed in section "Numerical Analysis of Clinching Process for Different Values of the Friction Coefficient", Figs. 25, 26, 27, 28 and 29.

Modelling of Deformation Process of Hybrid Joints with Application of the Brittle Epoxy DRAGON

Results of numerical simulations in pull tests for the materials parameters included in Table 10 are presented in Figs. 66 and 67. The comparison between force–displacement curves obtained in experimental and numerical tests (Fig. 66) shows high consistency with the clinched joint experiments. In the case of the hybrid joint, there is a difference in displacement at the maximum force. This difference can be caused by the effect of the assumed adhesive layer parameters (e.g., the thickness of the real adhesive layer differs slightly from the medium value 0.15 mm assumed in numerical simulations), friction coefficients and other features. One can notice high conformity up to the maximum force. The difference occurs after the failure of the adhesive layer (which corresponds to the maximum force), when the experimentally obtained shear force is greater than the one determined numerically. This is the result of the clinched joint strengthening by the adhesive, which was not taken into account in numerical simulations.

Results of simulated shear test for 3 mm displacement of joined strips is shown in Fig. 67. The bending of the punch side sheet and large regions of maximum von Mises stress in the case of the clinched joint are observed. In the case of the hybrid joint, there are almost no geometrical changes in the joint and the areas of von

Table 10 Properties of sheet materials and adhesive layer

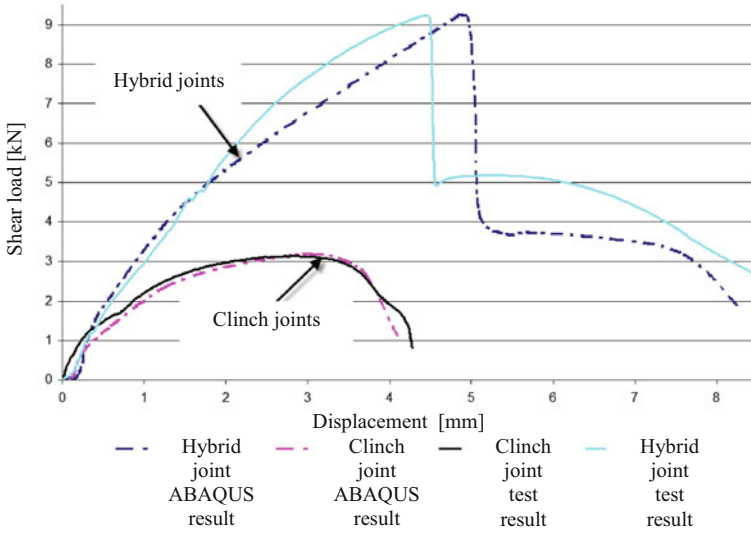| Joined material	Young modulus E_0 (GPa)	Poisson ratio v	Density ρ (kg/m^3)	Hollomon coefficients	
				K (MPa)	n
Steel	210	0.3	7800	690	0.246
Copper	127	0.3	8940	390	0.3
Adhesive material	Young modulus E_0 (GPa)	Kirchhoff modulus G_0 (GPa)	Density ρ (kg/m^3)	Shear strength σ_t^{max} (MPa)	Fracture energy G_{Ic} (J/m^2)
Dragon®	2	0.8	1150	20	750

Fig. 66 Comparison of experimental and numerical simulation results

Mises stress concentration are relatively small. In the hybrid joint, the load is carried by both the clinched joint and the adhesive layer, so the stress distribution is more uniform (it can be seen that the adhesive layer does not fail at this level of the shear force).

Modelling of Deformation Process of Hybrid Joints with Application of the Pattex® Repair Epoxy

The joints were built of the steel and copper adherends with properties specified in Table 10. The adhesive features are collected in Table 11.

Numerical simulations were performed using ABAQUS software with dynamic explicit approach. The blanks were meshed using C3D8R elements, involving in 10,816 elements for each blank and four elements in thickness direction. Presented results cover only the pull test results. The assumptions made in simulation process are shown in Table 12 and the simulation results are shown in Figs. 68, 69 and 70. The quadratic stress-based damage initiation criterion CSQUADSCRT for cohesive surfaces in general contact was used to estimate damage of the adhesive layer (Fig. 68); damage initiation occurs when the stresses satisfy the specified quadratic nominal stress criterion (3). The calculation were performed for the critical values: $\sigma_n^{max} = \sigma_t^{max} = \sigma_s^{max} = 6$ MPa.
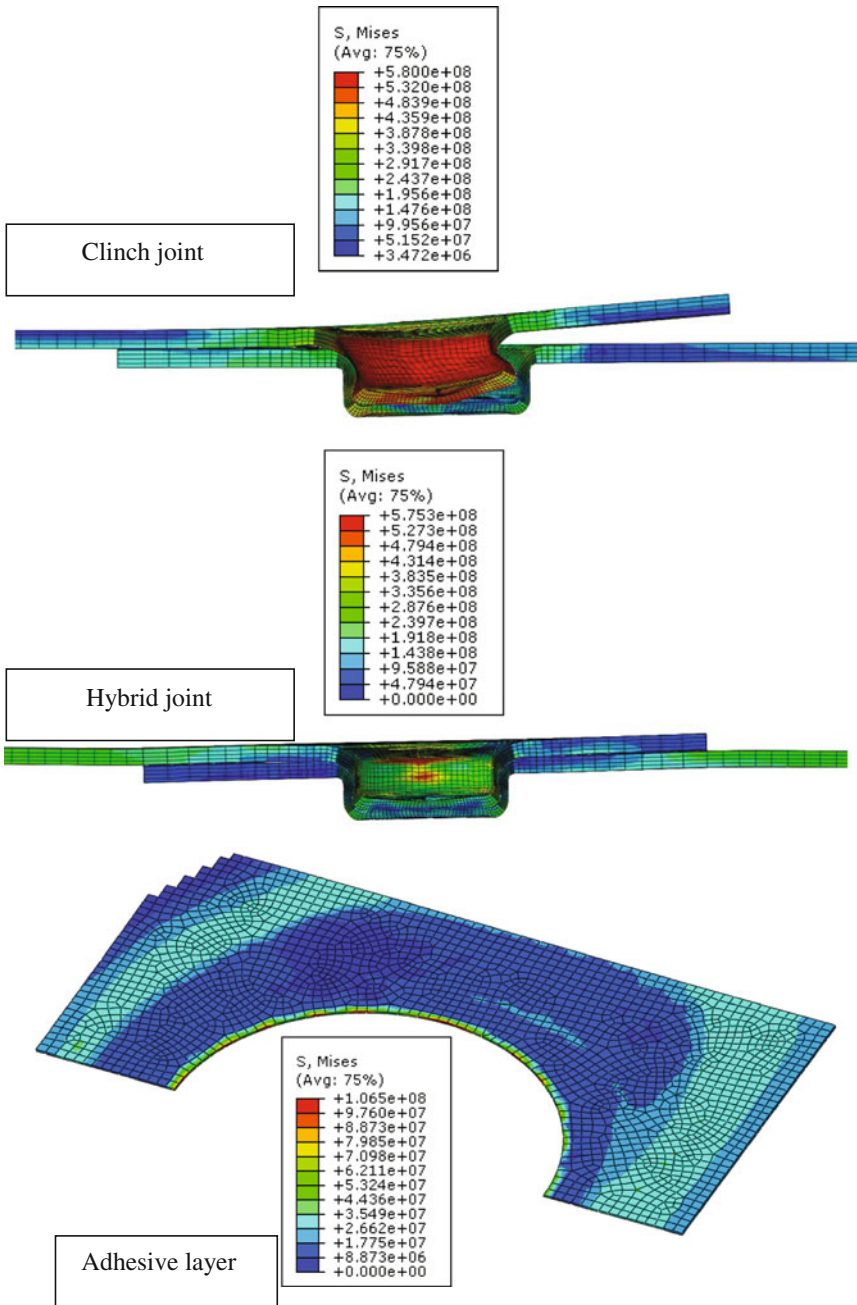
Fig. 67 Simulated the Huber–von Mises stress distribution (in Pa) during the shear process after a 3 mm displacement obtained for clinched joint, hybrid joint and adhesive layer in hybrid joint

Table 11 Properties of the adhesive layer

Adhesive material	Young modulus E_0 (GPa)	Kirchhoff modulus G_0 (GPa)	Density ρ (kg/m³)	Shear strength $\sigma_t^{\max}$ (MPa)	Fracture energy G_{Ic} (J/m²)
Pattex® Repair Epoxy	3	1.15	1050	6	275

Table 12 Contact conditions in the clinch joint cavity

Simulated stages of the process	Clinching before adhesive curing (A simulation)	Clinching after adhesive curing (B simulation)
Sheet drawing	Lack of friction between joined sheets; lack of cohesion properties	There are cohesion properties-friction 0.1 on the contact surfaces after adhesive layer failure
Anneal	Deletion of drawing stresses –it is in real process, when clamping the joint	No deletion of drawing stresses
Opening the clinching tools	Engaging of cohesion properties and then friction 0.1 on the contact surfaces after adhesive layer failure	No changes. Friction 0.1 on the contact surfaces
Joint failure	No changes in the contact definition	No changes in the contact definition

As it can be seen (Fig. 69) there is non-uniform stress distribution in A simulation, with stress concentrations around the clinch indentation. In case of B simulation the adhesive layer is destroyed in the clinched place and the destruction of the joint starts from the lap edges, like in an adhesive joint (Figs. 68 and 69).

Differences between experimental and numerical simulations are in the shearing force value. The experimental force values obtained in the pull test were in the range 4–4.5 kN, whereas the simulation results were 5–7 kN (Fig. 70). In experiments, greater force values were obtained for hybrid specimens prepared by procedure clinching before curing; inverse results were obtained in simulation.

The main reason of the discrepancy between experiment and simulation results, concerning hybrid specimen procedures (clinching before and after adhesive curing), are numerical simulation assumptions, but it should be noticed, that the differences between experimental results, obtained in these two applied procedures, are small. So, it is difficult to establish simulation conditions satisfying exactly experiment requirements. The presented simulation is only a trial of possible simulations by FEM, but the simulation assumptions should be discussed and corrected in future investigations.
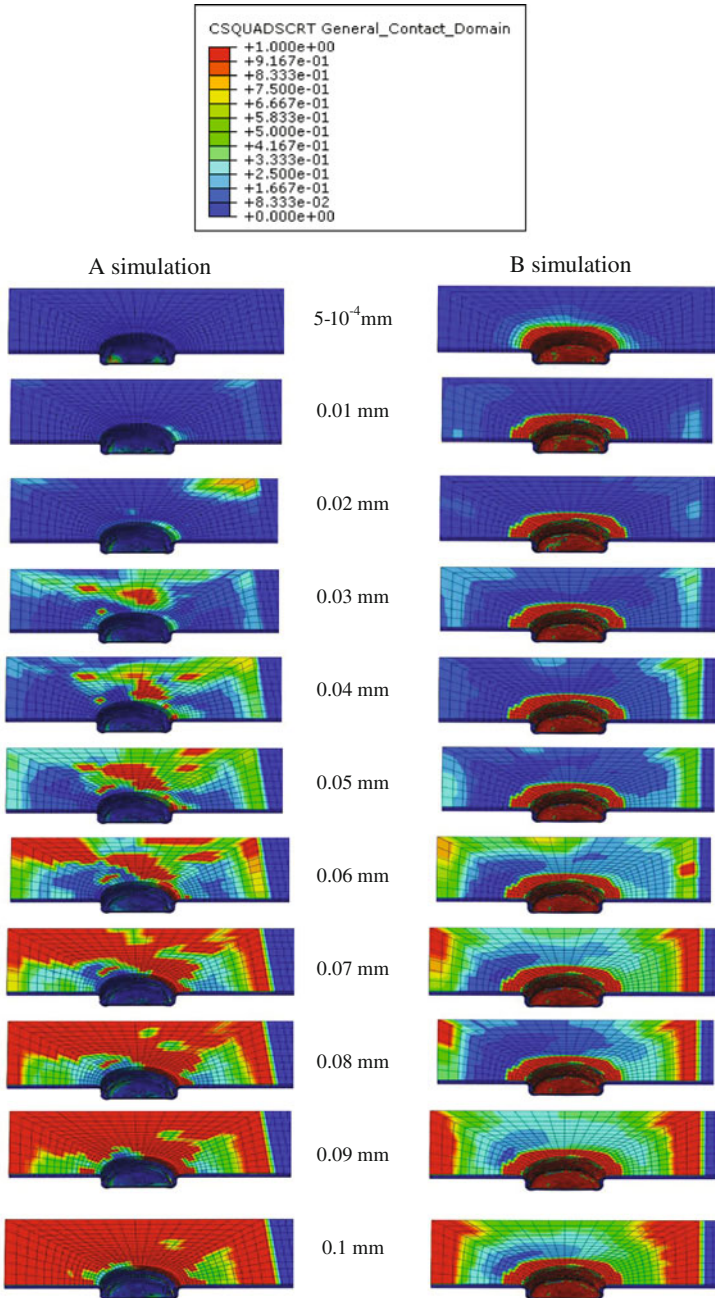
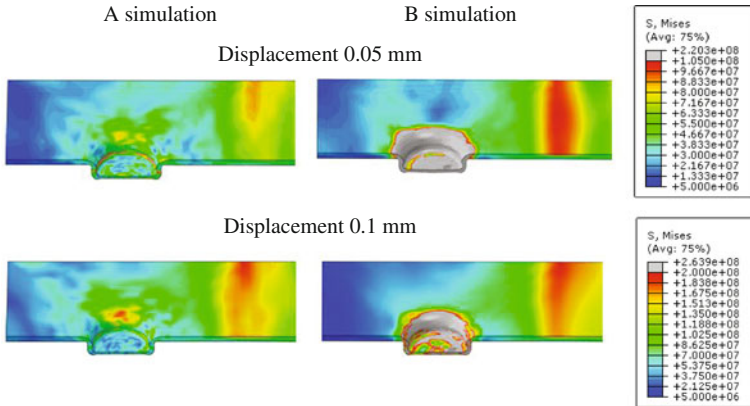**Fig. 68** Stages of adhesive layer failure in the pull process

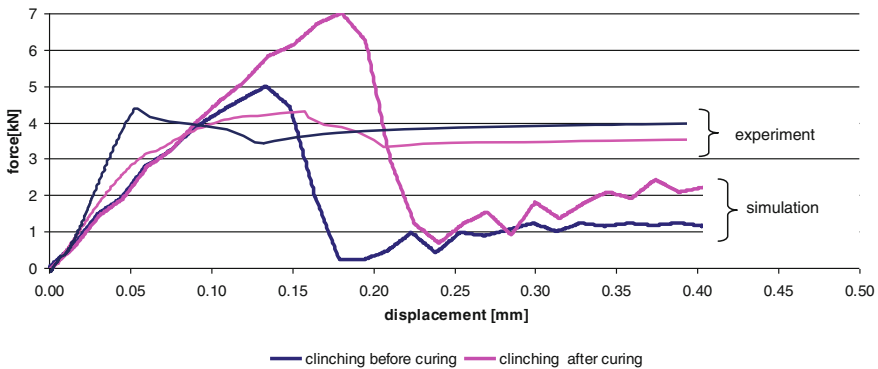**Fig. 69** The von Mises Stress distribution at the upper sheet during the pull test of the hybrid joints

Fig. 70 Simulated separation force evolution in the pull test—comparison between: clinching before curing and clinching after curing

Summary and Conclusions

Usage of cured adhesive is favourable for the clinched joint. Adhesive causes the increase of the clinch joint strengthand energy absorption.

Methodology of specimen preparation—clinching before adhesive curing—is more effective for the clinchedjoint performance than methodology—adhesive curing before clinching. Adhesive layer can be like a lubricantduring clinching and it can facilitate forming the clinch indentation, and then after curing, it gives strong adhesiveforces between sheets in the clinch cavity. The technique of clinching before adhesive curing create also more stiffjoints up to the maximum of the force-displacement diagram. Also the greater separation force was obtained forspecimens prepared by adhesive curing before clinching.

References

1. Varis J, Lepisto J (2003) A simple testing-based procedure and simulation of the clinching process using finite element analysis for establishing clinching parameters. Thin Walled Struct 41:691–709
2. Varis J (2006) Ensuring the integrity in clinching process. J Mater Proc Technol 174:277–285
3. Varis JP (2002) The suitability of round clinching tools for high strength structural steel. Thin-Walled Struct 40:225–238
4. Oudjene M, Ben-Ayed L (2008) On the parametrical study of clinch joining of metallic sheets using the Taguchi method. Eng Struct 30:1782–1788
5. de Paula AA, Aguilar MTP, Pertence AEM, Cetlin PR (2007) Finite element simulations of the clinch joining of metallic sheets. J Mater Process Technol 182:352–357
6. He X (2010) Recent development in finite element analysis of clinched joints. Int J Adv Manuf Technol 48:607–612
7. Oudjene M, Ben-Ayed L (2009) Shape optimization of clinching tools using the response surface methodology with moving least-square approximation. J Mater Proc Technol 209:289–296
8. Nong N, Keju O, Yu Z, Zhiyuan Q, Changcheng T, Feipeng L (2003) Research on press joining technology for automotive metallic sheets. J Mater Proc Technol 137:159–163
9. Balawender T (2013) Analiza wybranych sposobów zwiększenia wytrzymałości połączeń klinczowych. Oficyna Wydawnicza Politechniki Rzeszowskiej, Rzeszów
10. Abe Y, Kishimoto M, Kato T, Mori K (2009) Joining of hot-dip coated high-strength steel sheets by mechanical clinching. Int J Mater Form 2(Suppl 1):291–294
11. Sadowski T, Balawender T (2011) Technology of clinch-adhesive joints. In: da Silva LFM, Pirondi A, Öschner A (eds) Hybrid adhesive joints. Advanced structured materials, vol 6. Springer, New York, pp 149–176
12. Balawender T, Sadowski T, Golewski P (2011) Experimental and numerical analysis of clinched and adhesively bonded hybrid joints. J Adhes Sci Technol 25:2391–2407
13. Balawender T, Sadowski T, Kneć M (2011) Technological problems and experimental investigation of hybrid: clinched—adhesively bonded joint. Arch Metall Mater 56:339–446
14. Balawender T, Sadowski T, Golewski P (2012) Numerical analysis and experiments of the clinch-bonded joint subjected to uniaxial tension. Comput Mater Sci 64:270–272
15. da Silva LFM, das Neves PJC, Adams RD, Spelt JK (2009) Analytical models of adhesively bonded joints—part I: literature survey. Int J Adhes Adhes 29:319–330
16. da Silva LFM, das Neves PJC, Adams RD, Spelt JK (2009) Analytical models of adhesively bonded joints—part II: comparative study. Int J Adhes Adhes 29:331–341
17. Pocius AV (1997) Adhesion and adhesives technology. Hasner, New York
18. Adams RD, Comyn J, Wake WC (1997) Structural adhesive joints in engineering, 2nd edn. Chapman & Hall, London
19. da Silva LFM, Öchsner A (eds) (2008) Modelling of adhesively bonded joints. Springer, New York
20. da Silva LFM, Öchsner A, Adams RD (eds) (2011) Handbook of adhesion technology. Springer, New York
21. He X (2011) A review of finite element analysis of adhesively bonded joints. Int J Adhes Adhes 31:248–264

22. Barnes TA, Pashby IR (2000) Joining techniques for aluminium spaceframes used in automobiles part II—adhesive bonding and mechanical fasteners. J Mater Process Technol 99:72–79

23. Pereira AM, Ferreira JM, Antunes FV, Bártolo PJ (2010) Analysis of manufacturing parameters on the shear strength of aluminium adhesive single-lap joints. J Mater Process Technol 210:610–617

24. Pirondi A, Moroni F (2011) Science of clinch-adhesive joints. In: da Silva LFM, Pirondi A, Öschner A (eds) Hybrid adhesive joints. Advanced structured materials, vol 6. Springer, New York, pp 109–147

25. Banea MD, da Silva LFM (2009) Mechanical characterization of flexible adhesives. J Adhes 85:261–285

26. Higgins A (2000) Adhesive bonding of aircraft structures. Int J Adhes Adhes 20:367–376

27. da Silva LFM, Pirondi A, Öschner A (eds) Hybrid adhesive joints. Advanced structured materials, vol 6. Springer, New York

28. Sadowski T, Kneć M, Golewski P (2010) Experimental investigations and numerical modelling of steel adhesive joints reinforced by rivets. Int J Adhes Adhes 30:338–346

29. Sadowski T, Golewski P, Zarzeka-Raczkowska E (2011) Damage and failure processes of hybrid joints: adhesive bonded aluminium plates reinforced by rivets. Comp Mater Sci 50:1256–1262

30. Sadowski T, Kneć M, Golewski P (2014) Spot welding-adhesive joints: modelling and testing. J Adhes 90(4):346–364

31. Moroni F, Pirondi A, Kleiner F (2010) Experimental analysis and comparison of the strength of simple and hybrid structural joints. Int J Adhes Adhes 30:367–379

32. Sadowski T, Balawender T, Śliwa R, Golewski P, Kneć M (2013) Modern hybrid joints in aerospace: modelling and testing. Arch Metal Mater 58(1):163–169

33. Sadowski T, Golewski P, Kneć M (2014) Experimental investigation and numerical modelling of spot welding—adhesive joints response. Compos Struct 112:66–77

34. Geiss PL, Koetter MP, Presser M, Raudonat D (2010) Hybrid Joining with pressure sensitive adhesives. http://www.pstc.org/files/public/TeCH33Papers/

35. Brockmann W, Geiss PL, Klingen J, Schroeder B (2008) Adhesive bonding—materials. Applications and Technology. Wiley-VCH, Weinheim

36. Hammel V, Roelandt JM, Gacel JN, Schmidt F (2000) Finite element modeling of clinch forming with automatic remeshing. Comput Struct 77:185–200

37. De Paula AA, Aguilar MTP, Pertence AEM, Cetlin PR (2007) Finite element simulations of the clinch joining of metal sheets. J Mater Process Technol 182:352–357

38. Needleman A (1987) A continuum model for void nucleation by inclusion debonding. J Appl Mech 54:525–531

39. Tvergaard V, Hutchinson J (1992) The relation between crack growth resistance and fracture process parameters in elastic-plastic solids. J Mech Phys Solids 40:1377–1397

40. Postek E, Sadowski T (2011) Assessing the influence of porosity in the deformation of metal-ceramic composites. Compos Interfaces 18:57–76

41. Hilleborg A, Modeer M, Perterson PE (1976) Analysis of crack formation and crack growth in concrete by means of fracture mechanics and finite elements. Cem Concr Res 6:773–781

42. Hooputra H, Gese H, Dell H, Werner H (2004) A comprehensive failure model for rashworthiness simulation of aluminium extrusions. Int J Crashworthiness 9:449–464

43. Lemaitre J, Chaboche J (1978) Aspect phenomenologique de la rupture par endommagement. J Mech Appl 2:317–365

44. Sawczuk A, Sadowski T (1983) On anisotropic continuous damage of plates in flexure. Eng Struct 5:234–238

45. Sadowski T (1991) Deformation damage theory of materials and its application to the analysis of the deformation process of square plates. Arch Appl Mech 61:449–491

46. Sadowski T (1997) Thermodynamic approach to constitutive modeling of semi-brittle ceramics. Comput Mech 20:150–155

47. Sadowski T, Osina K (2008) Stress induced damage theory in application to modelling of matrix cracking in laminate polymer composites. Comput Mater Sci 43:51–59
48. Campilho RDSG, Pinto AMG, Banea MD, da Silva LFM (2012) Optimization study of hybrid spot-welded/bonded single lap joints. Int J Adhes Adhes 27:86–95
49. Campilho RDSG, Banea MD, Pchavres FJ, da Silva LFM (2011) Extended finite element method for fracture characterization of adhesive joints in pure mode I. Comput Mater Sci 50:1543–1549